POLITECNICO DI MILANO

Facoltá di Ingegneria Industriale

Corso di laurea in Ingegneria Aeronautica

Preliminary design of a test-rig for ORC turbine blades enclosed in a dense gas Ludwieg Tube

Relatore: Prof. Alberto Guardone
Co-relatore: Prof. Piero Colonna

Autore: Paolo Repetti 730627

Anno accademico 2010-2011

2

Contents

List of Figures

List of Tables

Summary

The harmful influence of fossil fuel on the environment urges to exploit renewable heat sources such as solar radiation, biomass and geothermal heat. In this view Organic Rankine Cycle is an attractive option for small to medium-scale application. The characteristics of organic fluids used in this kind of cycles are completely different from that of steam and therefore it is mandatory to impose our understanding of their behavior in order to improve the design of each component of the cycle. In this view the present work presents a preliminary design of a Ludwieg tube type facility that has the task to improving the design of the blades of ORCs turbine and to validate numerical codes.

The proposed test-rig was designed as a modification to an existent facility, FAST [36], used mainly for detecting of rarefaction shock waves. Despite its relative small footprint ($\approx$9x1 m) the FAST can ensure useful test time up to 0.25 s. An analysis of the behavior of the proposed facility has been conducted for different organic fluids. The expected flow over a six blade cascade placed in the test chamber was simulated with a dense gas inviscid CFD code and compared with periodic solution on the same blade (available in literature). The comparison show considerable differences due to spurious shock waves avoidable only by using porous tailboards [31].

The facility has been designed primarily for measurements with particle image velocimetry. In the last sections of this work several parameters like velocity and temperature relaxation time have been computed and compared with values coming from air experiments. Thanks also to the complexity of the organic testing fluid (and so to its low speed of sound) only one run seems to be necessary to obtain a large enough sample of the flow field necessary to obtain an accurate ensemble average. Results confirm the possibility of using a laser-based measurement technique in the facility.

Sommario

L'utilizzo massiccio di combustibili fossili nella produzione di energia provoca continui danni all'ambiente, per questo é necessario essere capaci di sfruttare nuove e pulite fonti di energia come quella solare o quella proveniente da biomassa e fonti geotermiche. Il ciclo Rankine organico in quest'ottica é un'ottima alternativa che, per piccole-medie applicazioni, si sta sempre piú affermando nel mercato internazionale. Le caratteristiche dei fluidi organici utilizzati sono completamente differenti da quelle del vapore, é quindi necessario conoscere al meglio possibile il loro comportamento in modo da migliorare la progettazione di tutti i componenti del ciclo.

Questa tesi propone un progetto preliminare di un tubo di Ludwieg per misure su schiere piane di turbine di cicli ORC utilizzando la tecnica della particle image velocimetry (PIV). Esso é pensato come una modifica a un esistente tubo di Ludwieg giá presente a TU Delft chiamato FAST [36] l'obbiettivo é quello di utilizzare il maggior numero di suoi componenti a partire dal serbatoio di bassa pressione e dalla valvola ad apertura veloce.

Dopo una breve introduzione, nel capitolo 2 si é cercato di arrivare a un primo dimensionamento della camera di prova (124x170 mm), presentando alcuni problemi che possono incorrere in questi esperimenti e evidenziando le scelte che andranno fatte in fase di progetto. Nel capitolo successivo vengono analizzate le due configurazioni proposte (con e senza divergente prima della camera di prova) mediante un'analisi 1-D. Grazie al basso valore della velocitá del suono nei fluidi investigati (MDM, PP5, Pentane) i valori del tempo di prova sono da ritenersi sufficienti: 0.25 s con un tubo di carica di 16 m nella prima configurazione e da 0.098 a 0.25 s (a seconda del fluido utilizzato) con un tubo di carica di 7 m nella seconda configurazione.

Successivamente é stato effettuato un confronto tra una simulazione 2-D inviscida della camera di prova con all'interno una schiera di 6 pale e una simulazione periodica [37], anch'essa inviscida, della stessa pala. A causa della riflessione delle onde d'urto sui contorni solidi della camera di prova le differenze si sono rivelate considerevoli, evidenziando la necessitá per questo tipo di esperimenti di ricorrere a tailboard porose. Infine sono stati calcolati i tempi di rilassamento delle particelle utilizzate per la PIV, degli indicatori che ci hanno permesso di stimare l'affidabilitá delle nostre misure, essi sono risultati comparabili a quelli riscontrabili in un esperimento avente l'aria come fluido di prova il che é sicuramente confortante.

Chapter 1

Introduction

1.1 Background & Motivation

The strong economic growth that large part of the world encountered during the last two centuries was made possible also by large scale utilization of fossil energy source. The current depletion of easily accessible fossil energy reserves as well as their deleterious effect on the environment enhance, increase the need of being able to exploit renewable energy source such as solar radiation, geothermal heat or biomass.

In this view organic Rankine Cycle (ORC) technology already takes a quite large part of the renewable market. Since it has relevant differences with classic steam Rankine Cycle, ORC component has different design criteria; moreover, it's clear that since ORC is a quite young technology there is large margin for improvement.

One of the main component of Rankine Cycle is the turbine, ORC turbine present huge differences respect to classic steam turbine, higher outlet Mach number, smaller dimensions, less number of stages are just some of the major differences. These are mostly related to the different thermodynamic behavior of the organic fluids used in ORC respect to the ideal gas behavior of the steam, so it's clear how is necessary develop specific tools (numerical and experimental) that could lead in an improvement in the design of this kind of blades.

1.2 Organic Rankine Cycle

The Organic Rankine cycle (ORC) is a Rankine cycle in which an organic working fluid is used instead of water-steam (e.g., a straight chain or aromatic hydrocarbon, fluorohydrocarbon, perfluorocarbon or a siloxane [1, 2, 4]). It gives the possibility to use heat of small supply rate and low temperature level (starting from approximately 90 °C).

The use of organic fluid for small to medium power plant (from few kWe up to 1-2 MWe) involves considerable advantages, first of all the chance to choose a fluid that is best apt to the specific feature of the cycle. The shape of the saturation curve for this complex fluid tends to exhibit a positive slope in the region of the expansion (figure 1.1), this allows the use of a regenerator without the risk of having a wet expansion with related problems to the turbine blades. Again, with the same power output, its lower density causes a lower enthalpy drop during the expansion this leads to bigger turbines with only one or two stages and with lower rotational velocity [2]. Usually a small specific work is

associated with a large expansion ratio, so ORC turbine have to deal with supersonic flow and possible shock waves.

The turbine is not the only component to take advantages in the using of organic fluids, also in the heat transfer process a better match between the heating trajectory of the working fluid and the cooling trajectory of the heat source can be obtained, thus increasing the conversion efficiency [5, 3]. Since saturation pressure is also much lower for organic fluids respect to water, the boiler then requires much thinner pipe-walls and does not require attending personnel for current regulations.

Adding to these benefits the fact that high efficiency for ORC can be reached with a very simple configuration (pump-boiler-single or double stages turbine-regenerator and a condenser), it is possible to understand how ORC may be a viable alternative in the energy field.
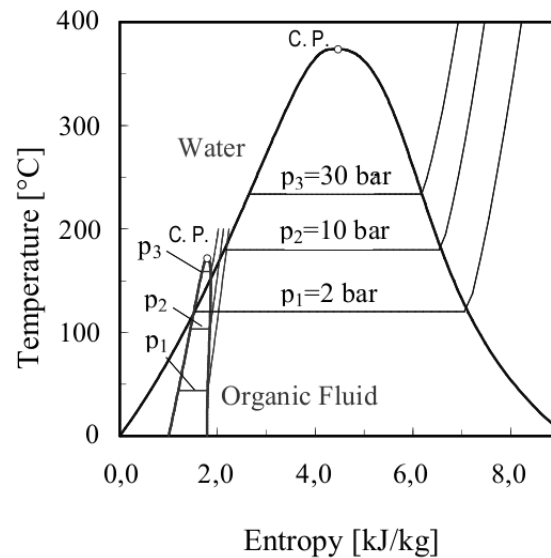
Figure 1.1: T-S Diagram for organic fluid and water.

For ORC it is also possible a supercritical configuration of the cycle is possible [3],in this case the heat transfer takes place at an average higher temperature (according to Carnot this increases efficiency) and during the expansion it is possible to reach a lower enthalpy value at peer pressure (figure 1.2).

Other useful advantages of the supercritical configuration are:

- The high density of the working fluid and the good overall heat transfer performance allows the dimensions of heat exchangers that are much smaller and more effective than traditional boilers. Due to the moderate increase of the pressure on the working fluid side with respect to boilers, the metal wall thickness would increase only moderately with respect to sub-critical boilers. On the other hand the total volume of the heat exchanger would be much smaller with respect to subcritical boilers and this would result in a considerable cost reduction.

- The smaller total volume of the heat exchanger would imply also a smaller footprint of the plant which is often a very desirable feature for this kind of installations and
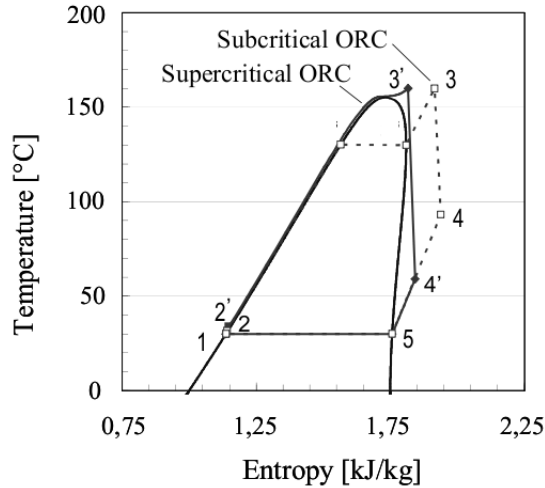
Figure 1.2: Sub- and supercritical ORC for R245fa [3].

in some cases it would allow for pre-assembly of the turbo-generator at the site of the manufacturer and delivery by truck. Experience of the manufacturers demonstrates that this is also an appreciable cost-reducing factor.

- The high density of the working fluid in the primary heat exchanger would also imply a much smaller fluid inventory with respect to sub-critical ORC. This in turn would imply a much faster response of the system to external perturbations. While this poses a challenge as far as the control design is concerned, on the other hand a successful control strategy could dramatically increases the ability to adapt to quick load changes.

At the present day no supercritical ORC system is available on the market. The reason is that the explorations of physical behavior in the supercritical region are just at the beginning, subcritical ORC contrariwise are widely used in electricity generation from low-grade geothermal heat reservoirs, from biomass, and the heat recovery from turbogas or reciprocating engines and industrial waste heat. Their market is growing at a rapid pace, with already hundreds of units and more than 1000 MWe installed. The use in the near future of ORC power systems coupled with solar concentrators, high-temperature fuel cells [6, 7] and for domestic cogeneration [8] is also very attractive, since they allow small-size plants and have low investment costs.

1.3 Dense Gas Flows

The peculiarity of that kind of cycles is that the expansion or compression process, as well as the heat transfer takes place close to or above the critical point of the working fluid, in this particular region (i.e. $0.9 < P/P_c < 1.2$ and $0.8 < T/T_c < 1.3$ or $P > P_c$ and $T > T_c$) the effect of long range and short range inter-molecular forces (van der Waals forces) starts to be significant and the ideal gas approximation is no more applicable.

	Chemical formula	M (g/mol)	$T_c(K)$	$P_c(atm)$
PP5	$C_{10}F_{18}$	462	565.2	17.3
PP10	$C_{13}F_{22}$	574	630.2	16.2
toluene	C_7H_8	92.1	617.7	20.7
MD_4M	$C_{14}H_{42}O_5Si_6$	459	653.2	8.0
D_5	$C_{10}H_{30}O_5Si_3$	371	619.1	11.4

Table 1.1: Chemical formulas, molecular masses and critical values of some organic fluids

The deviation from the ideal gas behavior is expressed in therm of $Z = pv/RT$, this thermodynamic behavior in turn lead to deviations in fluid dynamic quantities, those effect are mainly:

- *volumetric effect* adopting the ideal gas law leads to an underestimation of the density as we could see in fig. 1.3.

- *calorimetric effect* approaching in the dense gas region also the shape of the isoentropes and the specific heat deviate from the ideal gas prediction, fig 1.3.
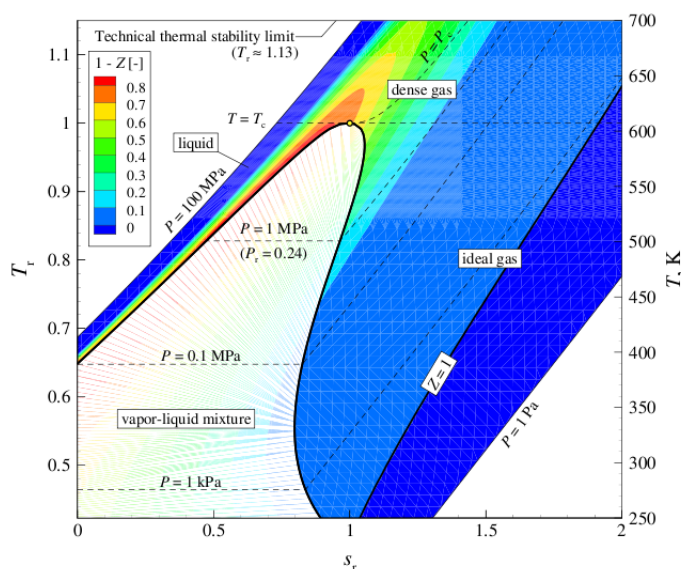
Figure 1.3: Deviation of volumetric properties from the ideal gas law for toluene [37].

Thompson [11] formally introduces the so-called fundamental derivative of gas-dynamics Γ:

$$\Gamma = 1 - \frac{v}{c}\left(\frac{\partial c}{\partial v}\right) \tag{1.1}$$

the value of Γ can be used to classify the gasdynamic behavior of a specific fluid. Following the work of Guardone and Colonna [12] increase in molecular complexity of the working fluid allows to reach progressively lower values of Γ:

- Flow with $\Gamma > 1$ everywhere is classified as Low Molecular Complexity (LMC), for this fluid real-gas effect is limited in qualitative variations respect the ideal gas behavior (for PIG model $\Gamma = (\gamma - 1)/2$).
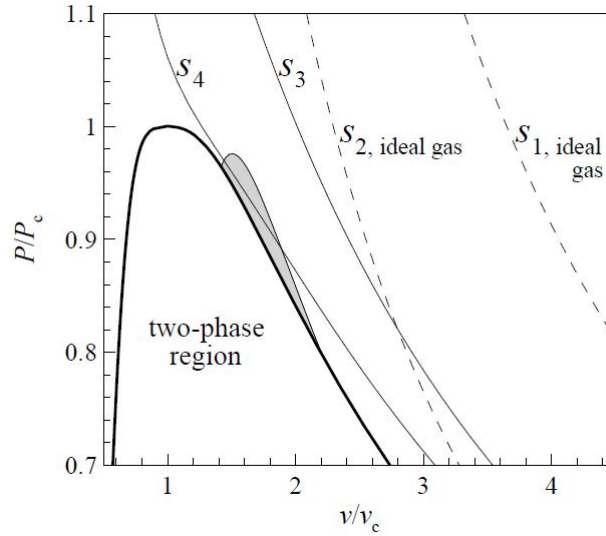
Figure 1.4: Isoentrope shape with ideal and real gas model for D6 [37].

- Flow with $0 < \Gamma < 1$ in a finite thermodynamic region is called High Molecular Complexity (HMC), it presents qualitative difference in fluid dynamic behavior in the dense gas region, close to saturation. Most notable is the increase in speed of sound upon a isoentropic expansion which can lead to a local decrease in the Mach number.

- Flow with $\Gamma < 0$ in a finite (small) thermodynamic region is called BTZ fluid, it presents non-classical gasdynamics behavior including rarefaction shock waves, this region is the shaded area in fig 1.3. One special feature of this region is that the isoentrope exhibits a region of concavity.

Fluid used in ORC is classified as HMC. In the process that takes place in the region close to critical point (i.e. expansion) forsaking the ideal gas approximation for a more accurate thermodynamic model may result in a better understanding of the flow field and then an increase in the efficiency of the cycle (for example thanks to a better design of the turbine blades).

For taking into account this behavior a large number of EOS (equation of state) have been developed, for LMC fluids it is possible to consider this effect by simply correcting the ideal gas law by a constant factor. For HMC and BZT fluids this does not lead to a satisfactory result. In [20] a large number of multi parameter EOS has been developed setting up the twelve fluid specific constant for MM, MD_4M, D_4 and D_5, this results in a better matching of thermodynamic properties.

In [19] two different expansions (subcritical and supercritical) for three different working fluids (steam, toluene and RU-123), they are investigated with two different thermodynamic models (PIG, SW). It is pointed out that using the PIG model for subcritical set-up leads to large deviation non uniformly distributed except for steam, for the most complex fluid,toluene, we have deviation of -20% in density, 25% in sound speed and 18% in velocity, and high error in the prediction in the flow rate of about -10% (steam). For the supercritical set-up the errors increase to -43% for density and 73% for sound speed

with a mass flow underpredicted by 14% out angle off by 2% and total pressure loss underpredicted by 30%. It is clear that errors of this magnitude could lead to a sub-optimal design of the cycle.

1.4   Scope of the Work

The scope of this work is to draw a preliminary design for a *dense gas Ludwieg Tube facility for linear blade cascade test*. Firstly a rough design of the facility is presented referring mainly to bibliography references and expertise opinion with particular attention to all the necessary equipment, in the second part the proposed configuration is analyzed in order to estimate several interesting test parameters (first of all the test time) and to predict the expected flow field in the test chamber. In the last section a short analysis of accuracy of the particle image velocimetry (PIV) measurement has been developed just to support the suitability of the organic fluids with PIV technique.

The main task of this facility is to reproduce a two dimensional flow over turbine blades. Firstly it could be used to validate any kind of numerical codes that have the task to predict dense gas flow over turbine blades, moreover it could be useful to support optimization work over this kind of blades and explore new possibility of improving ORC cycle (supercritical configuration).

The validation process has to be done gradually, starting from that phenomena more easily detectable up to the complex ones. The proposed procedure is the following:

- Step 1: Detecting position and angles of the shock wave that occur during the expansion (Schlieren visualization and PIV)

- Step 2: Comparison between the velocity profile obtained with the PIV measurements and the CFD solution

- Step 3: Comparison between pressure distribution over the blade

- Step 4: Boundary layer comparison

- Step 5: Heat transfer coefficient comparison

- Step 6: Turbulent quantities comparison

This procedure allows to a subsequent validation of the CFD code, the first three steps validate a generic inviscid solver, the following three steps validate a viscous and turbulent solver.

Chapter 2

Preliminary test rig design

Testing organic fluid flows through cascade cannot be conducted in standard facilities, long run times and enormous amount of fluid are necessary in standard wind tunnel. Moreover the opportunity to modify an existent facility already present at TU Delft [36] (FAST), with the consequent saving of money, suggests to apply the *Ludwieg tube principle* for the design of this dense gas facility.

A Ludwieg tube [13] is a transient facility that usually produces supersonic flows for short periods of time. The standard configuration (figure 2.1) [14] is composed by a large dump tank separated from the downstream end of a convergent-divergent nozzle and a long pipe by a diaphragm or a fast acting valve. Due to its special fluid dynamic features no devices are necessary to control the pressure or temperature during a run. The test gas is stored in a long charge tube. A fast opening valve separates the charge tube from the nozzle, the test section and the discharge tank.
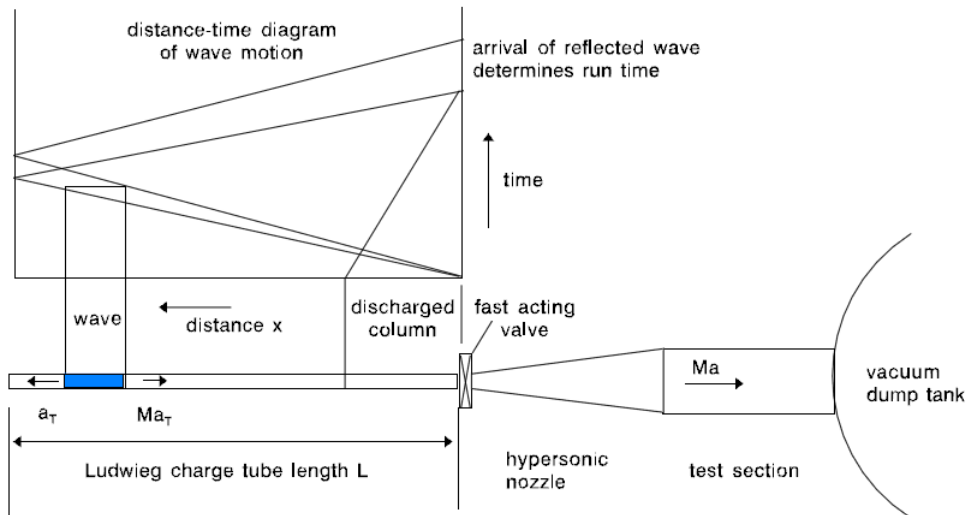

Figure 2.1: The operating principle and elements of an hypersonic Ludwieg tube setup

Initially, the pressure in the tube is high. When the diaphragm is ruptured or the

valve is open a shock wave propagates into the low-pressure region (the dump tank or often the atmosphere) and an expansion wave propagates into the high-pressure region. As this unsteady expansion propagates into the long tube, it sets up a steady subsonic flow toward the nozzle, which is accelerated by the nozzle to a supersonic condition. The valve is closed once the wave reflected by the end-wall reaches the nozzle throat and the test is finished. Thus the length of the tube and the speed of sound of the charge tube fluids determine the test run time.

At the closing of the valve, only a short column of the charge tube gas has been discharged. In order to start a new test the charge tube needs to be refilled and the dump tank must be evacuated. Typical run time are in the range between 0.1 and 0.5 seconds while the time interval between two run are between 200 and 600 seconds.

Another kind of facility of great interest is the blowdown wind tunnel [15] [17] [16]. It is also a transient facility, however in this case the gas is stored in a high pressure chamber separated from the rest of the tunnel by a valve. When this valve is open steady flow is generated through the test chamber for a time proportional to the pressure ratio between the low pressure and the high pressure vessel and to the volume of fluids.

Of special interest is the TROVA facility it is in fact the only blowdown test rig that has been thought for work with dense gases, it has an high pressure vessel with a capacity of 1 m^3 that through an isenthalpic throttling process pump the fluid in the test chamber that is suitable for nozzle and blade cascade, it discharges into a large area pipe and then into a low pressure vessel of area 5.6 m^3. The fluid under test is then pumped back into the high pressure vessel and brought to the desired thermodynamic condition (the limiting values of the plant are P=50 bar, T=400 $°C$).

Adopting a Ludwieg tube type configuration could lead to some advantages:

- extremely short startup time and shutdown time

- requires a smaller amount of fluid

- no regulation of temperature and pressure during run time

- no throttling valve upstream of the nozzle

- economy of the setup, no energy is required during the startup or the shutdown

- due to elimination of regulation valves, the entrance flow to the nozzle could be kept highly stable (low turbulence level in the test section)

The proposed facility has been thought as a modification of an existent facility built at TU Delft called FAST [36], it is a standard Ludwieg tube that has the task of reproduce rarefaction shock waves in BZT fluids. The intent is to reuse some part of this facility such as for example the fast opening valve and the low pressure plenum. The main mechanical components of the FAST are:

- a low-pressure vessel of approximately 1 m^3;

- a charge-tube consisting of 6 segments of about 1.5 m (these segments are connected by means of specially developed couplings);

- the so-called balance of plant consisting of a condenser, an evaporator, a vacuum pump;

- a custom-made fast-opening valve placed inside the low-pressure vessel: the FoV has an opening time of 4 ms at 360 $°C$ and has a built-in nozzle with adjustable throat area.
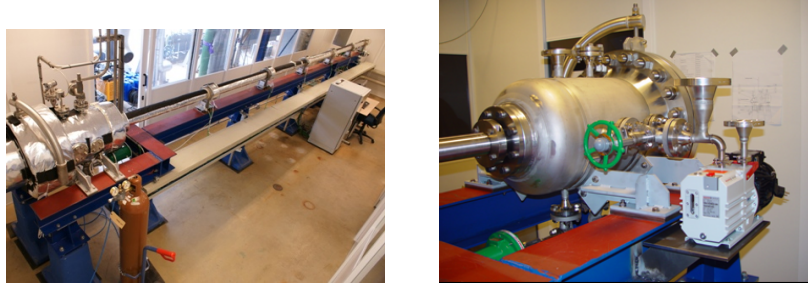
Figure 2.2: FAST-Flexible Asymmetric Shock Tube

This ORC Ludwieg tube presents some differences with standard Ludwieg tube, it could be an hybrid between a standard Ludwieg tube and a blowdown tunnel. It presents a long charge tube connected to the quiet chamber through a suitable fitting, then at the end of this chamber the linear blade cascade has been installed to discharge the fluids in a low pressure plenum, between the cascade and the plenum a fast opening valve (FOV) has been placed.
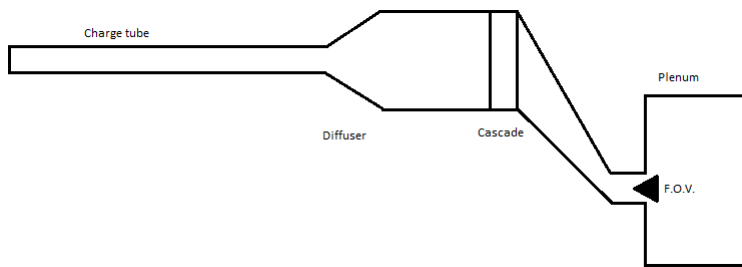
Figure 2.3: Conceptual representation of the Ludwieg tube for linear cascade testing

2.1 Operating principle

Starting from rest condition the facility is divided in two zone by the FOV, on the right the high pressure zone, on the left the low pressure zone that has to be low enough (respect to the right pressure) to choke the cascade. Once the valve has been opened a problem known in literature as Riemann Problem occurs [23]. Depending on the difference between the thermodynamic state between the left and the right side of the valve pressure perturbations propagate through the facility and in the low pressure plenum, in our situation we are dealing with an expansion fan that travels through the high pressure side and a shock wave that goes into the plenum.

If the pressure on the left side is low enough the cascade becomes chocked, therefore no perturbation could go back from the plenum, the expansion wave contrariwise travels along the facility until it reaches the connection between the tube and the test chamber. At this point, depending on the area ratio, two different situations could occur.

The most simple occurs when the area of the tube matches exactly the area of the test chamber, in this case the strength of the fan remains unchanged, then in the test section a steady flow occurs except for perturbations that arise from the change in the cross section (from circular to rectangular), these are easily softened using honeycomb grids before the cascade.

In case of cross section area of the pipe less than that of the test section the interaction with a monotonic area reduction produces transmitted and reflected rarefaction waves and other possible shock waves [24]. Depending on the magnitudes of the area reduction ratio and the incident rarefaction wave strength (or pressure ratio across the wave), see figure 2.5, the interaction will result in one of the four different postulated patterns in figure 2.1.

(a) Pattern A   (b) Pattern B

(c) Pattern C   (d) Pattern D
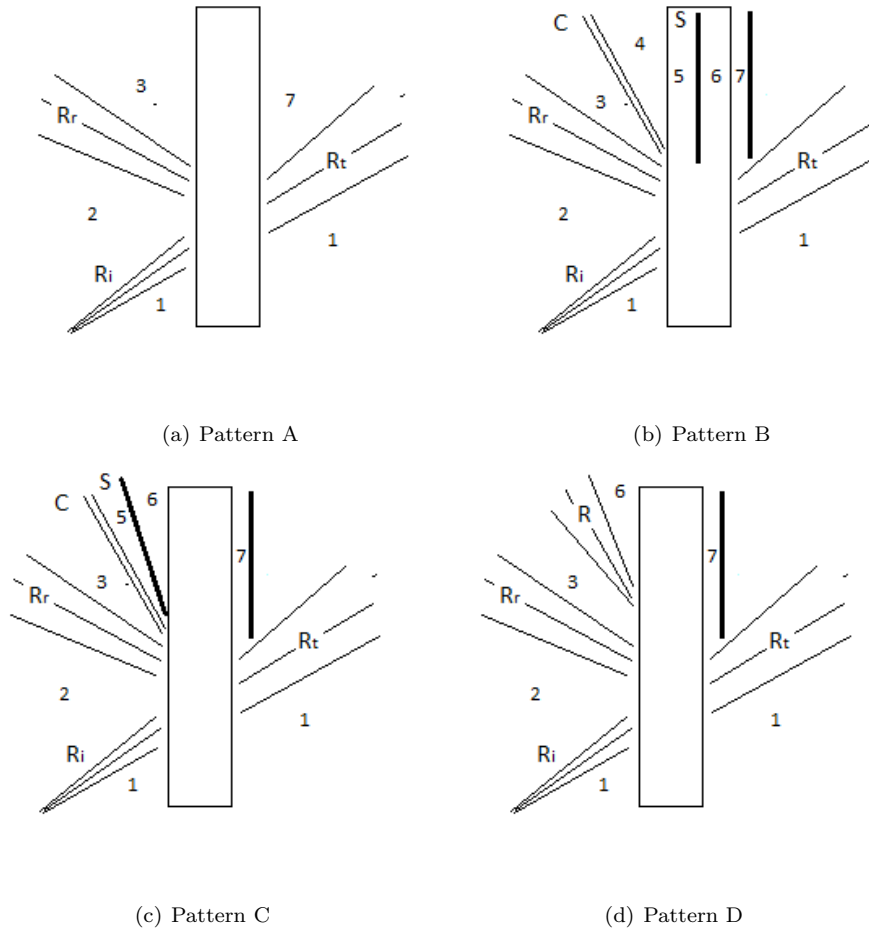
Figure 2.4: Four different quasi-steady wave patterns for the interaction of a rarefaction wave with an area reduction in a duct

In all four cases an expansion wave R_r is reflected backward by the area change, an upstream-facing shock wave appears also in the change area in pattern B or downstream of it in pattern C, whereas in pattern D one more rarefaction wave going backward appears. Owing to the existence of the shock wave in pattern B and C a contact discontinuity occurs.
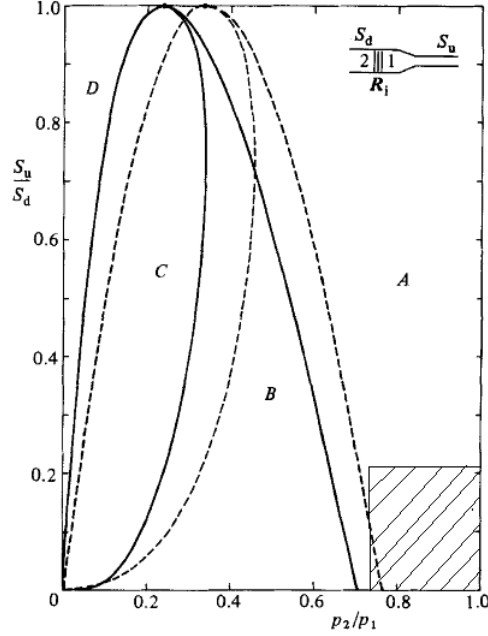
Figure 2.5: Domains and boundaries for wave patterns A, B,C and D, the continuum line refers to a politropic ideal gas with $\gamma = 1.4$, the dashed line to a politropic ideal gas with $\gamma = 1.1$, the shaded area is approximately the area of interest in our cases [24].

All of this process is initially non-stationary process, then a numerical solution is needed , however, as local transient motion subside, the flow will become quasi-steady. For an inviscid flow, the flow properties in region 1-7 (pattern A) are connected by the equation:

$$\begin{cases} s_1 = s_7 \\ u_7 = \int_{v_1}^{v_7} \frac{c(s,v')}{v'} dv' \\ h_1 = h_7 + \frac{1}{2} u_7^2 \end{cases}$$

(with $u_1 = 0$), for a steady one dimensional isentropic flow through an area reduction, is possible obtain the state 3 from the state 7 using the continuity and the energy equation:

$$\begin{cases} \rho_7 u_7 A_7 = \rho_3 u_3 A_3 \\ s_7 = s_3 \\ h_7 + \frac{1}{2} u_7^2 = h_3 + \frac{1}{2} u_3^2 \end{cases}$$

Region 2 lies between the incident and reflected wave, therefore the flow properties in this region are connected to the flow properties in region 1 and 3:

$$\begin{cases} s_1 = s_7 \\ u_2 = \int_{v_1}^{v_2} \frac{c(s,v')}{v'} dv' \\ u_2 = u_3 + \int_{v_3}^{v_2} \frac{c(s,v')}{v'} dv' \end{cases}$$

This completes the method of solution for obtaining all flow properties and wave strength for pattern A.

The solution for pattern A covers a limited range of strengths of the incident waves, the ratio p_7/p_1 start from 1 (for which there is no flow) to its minimum value where the

tail of the transmitted rarefaction wave becomes vertical (pattern B) and the flow entering the divergent is sonic. At this point a shock facing in the area changes, the flow is still resolvable adopting the well known Rankine-Hugoniot relations. For pattern C the shock wave is swept downstream by the oncoming supersonic flow, finally in pattern D it is replaced by a rarefaction fan and the contact discontinuity disappears.

The operating condition required for this facility refers to pattern A. The reflected fan starts moving through the cascade when it arrives at the inlet the same process (pattern A) occurs, the transmitted wave going into the vacuum tank and the reflected wave coming back to the divergent triggering the same process. The intensity of the reflected wave is gradually reduced since it becomes negligible, at this point steady flow moves towards the cascade and the test can begin. It lasts till the first transmitted wave has travelled the entire length of the tube and come back.

2.2   Subsonic test chamber design

Linear cascade test rig is not an easy task because of the difficulty in establishing truly periodic and two dimensional flow conditions at the midspan of the central blade of the cascade. Truly periodic flow field requires a large (infinite in the ideal case) number of blades, however because of mass flow and dimension restriction the cascade have to be made up of a small number of blades (5-9).
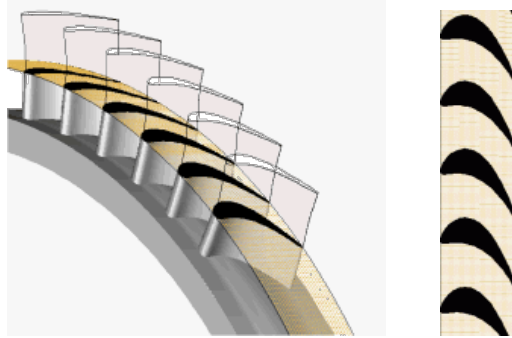
Figure 2.6: From a turbine rotor to a linear cascade

Because of the development of the boundary layer on the cascade tunnel side walls, all linear cascade flows are inherently three dimensional. In general, these effect are bigger in decelerating cascade (compressor cascade), the combination of small inlet boundary layers, high aspect ratios and high accelerations in fact are conditions which favor two dimensional flow conditions.

The velocity at the inlet of the cascade has to satisfy the conservation of mass, therefore it is fixed by the operating condition and the inlet to throat area ratio. In order to have accurate measurements a steady flow over the cascade has to be reached, assuming steady inlet condition this happen when the boundary layer over the blade reaches a steady state thickness, the growth time of the boundary layer is therefore another relevant parameter to take in account [26]:

$$\tau_b = \frac{\delta^2}{u} \approx 1.5\frac{L}{u} \qquad (2.1)$$

where δ is the thickness of the boundary layer u is the outlet velocity of the cascade and

L the chord. This time is in the order of $10^{-3}/10^{-4}$, therefore the boundary layer over the cascade could be assumed completely settled during the test.

Before we get into in the sizing of the test section, it seems appropriate to show the main features of some facilities for testing the steam turbine cascade (table 2.1). None of it are Ludwieg tube also because with steam the problem of using a small amount of fluid is not present, the VKI facility seems at the forefront especially for the small dimensions of the test section.

	VKI	Gorttingen	Braunschweig	Oxford
Type of facility	Blowdown	Suckdown	Closed loop	Blowdown
Test section height (mm)	180	353	427	420
Test section width (mm)	50	125	300	300
Upstream straight wall length (mm)	1000	2500	1550	800
Downstream guided wall length (mm)	200	650	250	290
Number of blade	10	10	7	7

Table 2.1: Geometric parameters of test section of four European facilities

2.2.1 Two dimensional flow conditions

The achievement of two dimensional flow at the midspan of the central blade of the cascade is closely related with the aspect ratio of the model blade,that has to be kept as high as possible. For supersonic outflow Mach number cascade the boundary layer undergoes an overall acceleration resulting in a thinning of the boundary layer and then in an effective divergence of the blade channel (until no shock wave is generated). In this case the boundary layer may undergo a thickening compared to its state in the throat, but since it is a thickening of an initial thin boundary layers its effect on the flow at the midspan appears to be small.

The best evidence of an effective spanwise divergence up to the throat is the recording of measured chocking Mach numbers in excess of the theoretical chocking Mach numbers for two dimensional flow. However, as demonstrated in a comparison between various cascade wind tunnels with inlet duct to blade height ratios varying from 5 to 20, this does necessarily affect neither the blade losses nor the outflow angle in a significant manner [27].

To keep three dimensional effect small, the relative inlet boundary layer thickness must be small. It is therefore essential to keep inlet duct to blade height ratio small and the aspect ratio high. Based on a limited amount of cascade data Sieverding in [28] proposed minimum aspect ratio of 1.6, Jouini in [29] observes that this value is satisfactory only at the design incidence, although for high value of off-design incidence ($\approx 14.5°$) this value is not acceptable.

Clearly as long as only the study of the first stage of the stator is the purpose of our experiments, it is not necessary investigate a high off-design incidence, however since the facility will be designed to have the greatest possible flexibility an aspect ratio of 2 seems a good value, that may allow also the testing of rotor stages and stator stages beyond the first. The height of the test section is related to the number of blades that have to guarantee periodic flow, this varying from 5 to 10.

Some wind tunnels are provided with movable walls, for example the EGG at the DLR Goettingen [17] has a variable height test section in the range of 240-400 mm, this set-up

allows a better fit to a better fit of the cascade with the upper and lower wall, however the same effect could be obtained scaling the cascade (as long as dynamic similarity can be considered satisfied).

Other devices often present in such wind tunnels are boundary layer suction devices. Considering that the flow at the inlet may come from a divergent where the adverse pressure gradient introduces a large thickening of the boundary layer, this devices seems necessary. Connecting the test section just upstream of the inlet of the cascade with the low pressure plenum the suction system doesn't require any additional power.

2.2.2   Cascade outlet flow periodicity

Shock and expansion waves generated inside the cascade interfere with the boundaries limiting the cascade exit flow field and deteriorating the flow periodicity. It is well known that in supersonic flows waves are reflected with the same sign and the same absolute flow turning angle from a plane solid walls. On the other hand, along open boundary, the condition of a constant static pressure along the boundary must be met, therefore a compression wave meeting an open boundary will be reflected as an expansion wave of equal intensity with the same absolute pressure change.

Figure 2.7: The shock wave coming out from the trailing edge of each blade, bouncing against the upper wall and reflected over the next blade (Schlieren picture [33])

In linear cascade the reflected wave could disturb the flow field of the blade of interest, however since solid boundaries and open jet produce wave reflections having opposite characteristic, there is a possibility of eliminating wave reflections by mixing open and solid boundaries. The inclined flow behind an oblique shock waves meets the perforated wall and produces a pressure drop when it flows through the wall, if this drop is equal to the pressure rise through the main oblique shock wave the condition of no reflection is obtained.

This technique is widely used in cascade wind tunnel by adopting porous tailboards [30], however the problem is very case-specific and the correct size of the openings depends upon the shape of the openings, the thickness of the wall boundary layer, the Mach number and the flow angle. In [31] [32] the effect of an optimized tailboard has been evaluated on a supersonic linear cascade in terms of outlet periodicity, the result confirms that tailboards reduce the end-wall interference not only at the design conditions but also in a range of different outlet Mach number and flow angle.

Moreover tailboards are mandatory in this type of test, in fact their angle of inclination respect to the blade trailing edge is strictly connected with the pressure ratio over the cascade. As discussed later in fact, in order to respect the same pressure ratio of the real turbine the tailboard has to be inclined as the streamline coming out from the blade trailing edge (easily predicted throughout a CFD periodic simulation).

2.2.3 Test section dimension

The size of the test section should not be separated from the measurement technique. To have an accurate measurement the geometry should not be too small. The more critical dimension of the cascade is clearly the throat, then fixing from expertise experience a minimum dimension of 5-3 mm to achieve good accuracy it is now possible to go back to an approximate sizing.

For a first sizing of the test section a commercial blade (Biere), that has been widely studied in [37], has been taken as reference. Its throat height is around 5 mm then a scale close to 1:1 seems to be necessary for testing this type of blade, the blade chord is around 60 mm. The first proposed dimensions based on this geometry are:

- width = 124 mm

- height = 169.2 mm (five blades) or 253.8 mm (seven blades)

This dimension minimizes the scale effect, however the area ratio between the tube and the inlet of the cascade could be very low (especially in the case of seven blades) then this may present other problems, first of all, the smaller the area ratio is the longer the diffuser has to be, and the thicker the boundary layer at the inlet becomes, moreover while pass through a divergent all disturbances are inevitably amplified. The dimensions then have to be a compromise between scale effect, PIV accuracy, area ratio between charge tube and test section.

2.3 Charge tube design

The charge tube dimensions have to be chosen carefully, as we'll see in the next section the flexibility of the facility depends strongly on the radius of the tube, moreover the useful run time is strictly related with its length. Clearly the tube cross section and length should not be too large, firstly for reasons of cost (primarily of the fluids under test), secondly

with too large cross section convection could be established inside the tube leading to a non-uniform flow towards the cascade.

Between the test section and the charge tube, since they are of different shape, a link is necessary, it has to be a divergent in fact it is expected that the charge tube have a lower cross section respect to the test chamber. A diverging link is particularly problematic, in fact the small perturbation crated in the charge tube during the starting process becomes bigger passing through this link.

As said before this is a critical decision that has to come from a trade off between the problems listed above. The original set-up provides a tube of dimension much lower than test section, according to this consideration also a tube of cross section equal to the test section has been considered in the subsequent analysis.
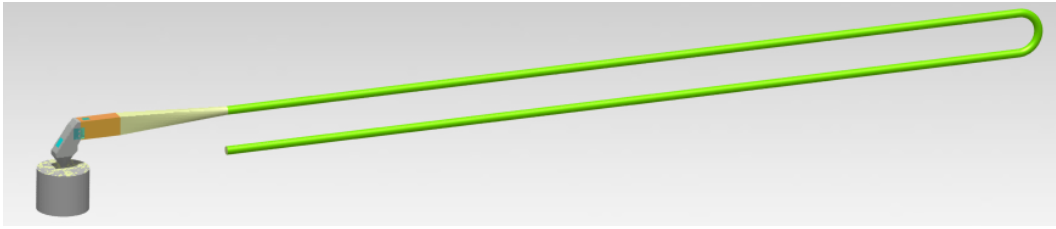
Figure 2.8: Rough CAD design of the proposed facility

2.4   Equipment

2.4.1   Laser & Windowing

Firstly the characteristic of the main component are listed:

Pco.dimax CCD camera	
Resolution	2016 x 2016 pixel
Frame rate	1100 fps (full resolution)
	4000 fps (half resolution)
Dynamic range	12 bit
Exposure time range	2 μs-1 s
Dual power laser	
Power	2 x 22.5 mJ
Frequency	1000 Hz
Wavelength	527 nm

Table 2.2: Laser and camera data sheet

PIV measurements technique requires optical access, either for illuminating the field of interest, either for recording the light scattered from the particles illuminated. For this reason the test chamber requires at least one window for the camera and one window for the laser sheet.

The interested area in case of cascade testing is the nozzle between the two central blade and the region downstream of it. Since the typical nozzle of ORC turbine is very curved it is not possible to illuminate the whole field of interest with only one laser beam

(figure 2.4.2). In fact, illuminating from the front or from the rear part of the cascade will certainly put respectively the inlet or the outlet of the nozzle in a shadow region. One solution is adopting transparent blade, however its high curvature induces too high refraction effect on the laser sheet [35].
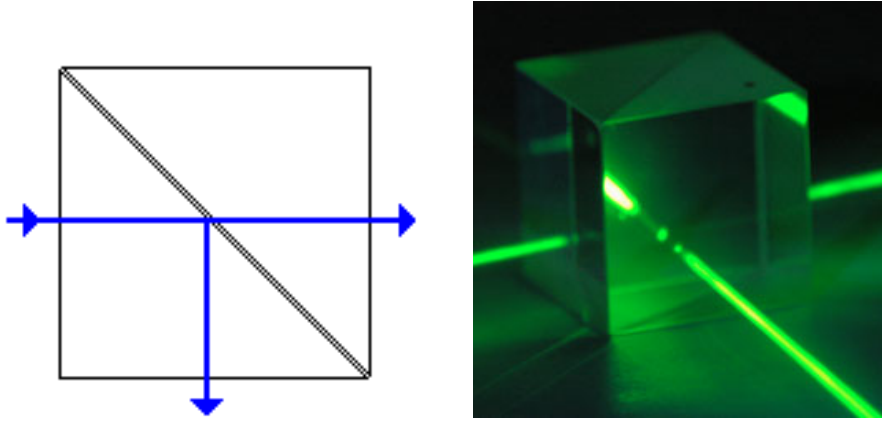
Figure 2.9: Beam splitter

The proposed solution, to avoid the use of two lasers, is to use a beam splitter 2.4.1, this device allows to split the laser beam in two different beams of half intensity, than using a mirror system it is possible to deviate each laser beam in two different directions in order to illuminate all the field of interest. This device is not without complications, the intensity of the beam in fact is related with the intensity of the light scattered by the particle, in the case of low-intensity laser it could occur that the particles are not visible by the CCD camera. The number of the beam splitted therefore has to be limited to two.

2.4.2 Seeding

Seeding procedure is a crucial operation for the success of the experiment, the particle size have to be small enough to follow the flow being measured but large enough to generate a strong scattered signal. Particle size, composition, density, shape and concentration are important factors when selecting seed particles.

The particle fidelity could be quantified by the relaxation time [35]:

$$\tau = \frac{4\rho_p d_p^2}{3c_d Re_d \mu_f} \tag{2.2}$$

where ρ_p is the particle density, c_d is the particle drag coefficient, Re_d is the particle Reynolds number and μ_f is the flow viscosity. When the relaxation time is high the particle fidelity is low.
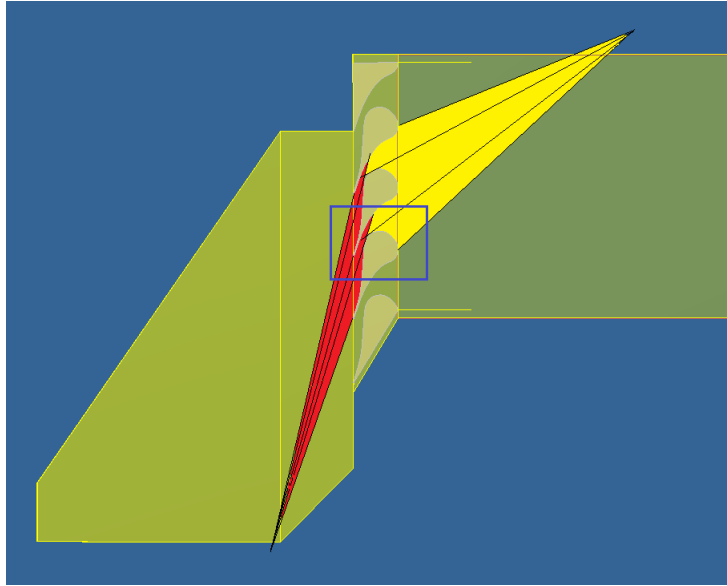
Figure 2.10: Illumination of the field of interest: the yellow area is the front laser sheet, the red area is the rear laser sheet and the blue rectangle is the field of interest

The particles proposed for this kind of experiment are solid titanium dioxide (TiO2) with a nominal crystal size of 50 nm and a bulk density of $\rho_p = 200 kg/m^3$ which are chosen for their high resistance to thermal break-down and for their high availability (e.g. toothpaste).

The input of the particles into the facility is provided by a tool called *cyclone*. This is a cylindrical box with the particles inside, blowing the working fluids inside this tool from the lateral wall the particles are set in motion and then begin to move in circle, obviously the bigger (and heavier) particles will turn outside. Therefore sucking the fluids from the center of the box enables us to take only the lighter particles and not placing into the charge tube agglomerated particles. It is primary importance to avoid any contamination of the working fluids with air.

The fluid seeded sucked from the cyclone going directly to the charge tube. Another pipe provides the charging of the tube with pure fluids. With this set-up it is possible to dose the quantity of the particles in order to obtain the correct concentration. In this case trial and error procedure is needed and therefore the repeatability of the experiment is a key point. The feeding inlet is at the bottom of the tube, in this case the particles will be pushed at the top by the incoming flow, in fact it is worth considering that not the total amount of the fluid is set in motion by the expansion wave.

Figure 2.11: TU Delft cyclone seeder

Chapter 3

Assessment of the design

In this chapter one-dimensional and two-dimensional CFD analysis has been carried out to predict the behavior of the facility. Both have been carried out using zFlow the in house code available at TU Delft coupled with the thermodynamic library FluidProp that collects a wide number of accurate EoS.
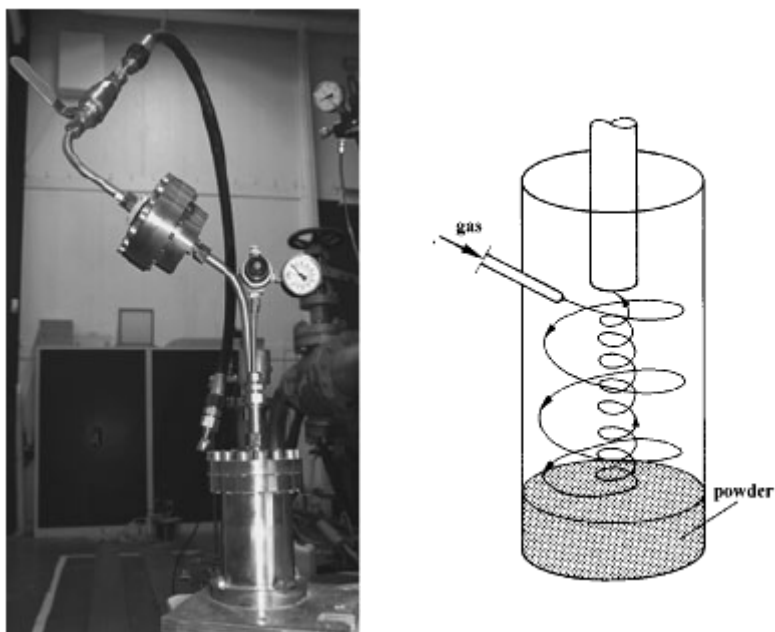
A first class of EoS are called Peng-Robinson-Stryjek-Vera (PRSV), it requires only the critical parameters and the acentric factor of the fluid. More accurate models are the so-called multiparameter EoS, for example Span-Wagner, it features the reduced Helmoltz energy $\Psi = \Psi/RT$ as a function of the reduced density, $\delta = \rho/\rho_c$ and the inverse of the reduced temperature, $\tau = T_c/T$. It overcomes the deficiencies of the cubic Eos (PRSV) being extremely accurate also in the vicinity of the critical point and has an excellent numerical stability compared with older multi-parameter EoSs.

ZFlow is a CFD program developed at TU Delft, it is an hybrid between finite element (FE) and finite volume (FV), the high-resolution upwind discretization is constructed on the basis of Roe approximate Riemann solver generalized to the case of arbitrary equations of state. A wide class of problem could be solved with this code, in this thesis the one-dimensional transient solver and the two-dimensional steady Euler solver have been widely used.

3.1 One dimensional transient analysis

The scope of this analysis is a better understanding of the starting process of the facility with different configuration and to obtaining initial estimates of some characteristic quantities especially the test time.

The CFD code solves the flow field forward in time starting from initial step condition. As integration scheme has been adopted a Runge-Kutta with two stages. The behavior of the facility has to be the one presented previously. However, since we are dealing with very particular fluids, before doing the facility simulation we have thought to explore the behavior of a rarefaction wave traveling through a diverging duct of dense gas and to compare it with the ideal gas behavior.

3.1.1 Dense gas pattern definition

Following the work of Gottlieb [24] the behavior of a expansion wave moving through an area change is addressed. The geometry adopted (figure 3.1) is a straight channel with

a divergent, the expansion wave is created starting from step initial condition. For the divergent the following smooth equation has been used to define its boundary:

$$r = exp(-log(\frac{A_s}{A_t})^{0.5}(\frac{L_d\pi}{2}sin(\frac{2\pi}{L_d}x) - x) - log((A_s/A_t)^{(L_tA_t)/(L_d)})) \qquad (3.1)$$

The mesh is composed of 1502 elements (in figure only one every twenty element is plotted) and it is refined with a gaussian function at the divergent and at the initial step.
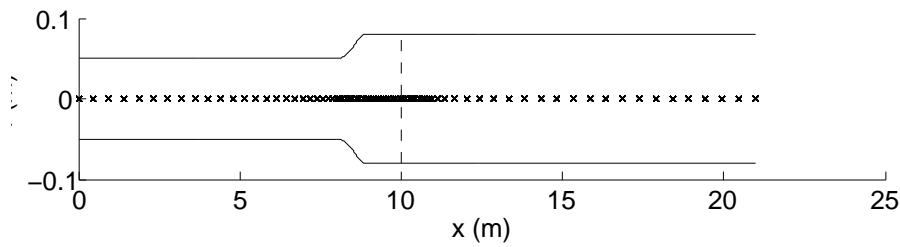
Figure 3.1: Geometry of one example case, the crosses are the mesh point, the dash line represents the initial location of the step

Firstly the pattern A is reproduced, the initial step condition states, the waves strength and the asymptotic solution is reported. Two different condition have been addressed, one with initial pressure and area ratio widely in the region of pattern A and one still in this region but close to the boundary with region B:

P_l	ρ_l	P_r	ρ_r	P_2/P_1	P_7/P_1	P_3/P_2	A_s/A_t
12	109.89	9.6	76.92	0.8951	0.8692	0.9806	1.5
12	109.89	8.4	65.93	0.8376	da det.	0.9059	4

Table 3.1: Initial states and waves strength for pattern A

The expansion waves gains power passing through the divergent, at the same time a low strength waves is reflected backward, the developing of steady flow after the passage of the reflected wave can be clearly seen (figure 3.1), note that the steady flow in the area change decelerates and its pressure rises as we expected from the classical behavior of a flow through a divergent.

In all the figures presented the shock wave that occurs due to the particular initial condition and travels to the right is not reported for clarity and because it has no relevance in this simulation, in figure 3.1 (b) the steep rise in the Mach number after the diverging is due to the contact discontinuity generated by the initial step condition. It doesn't occur in the real case,as for the non reported shock waves, because the valve is placed downstream to the cascade and both can't go upstream since the expansion wave choked the cascade.

(a) Pressure   (b) Mach
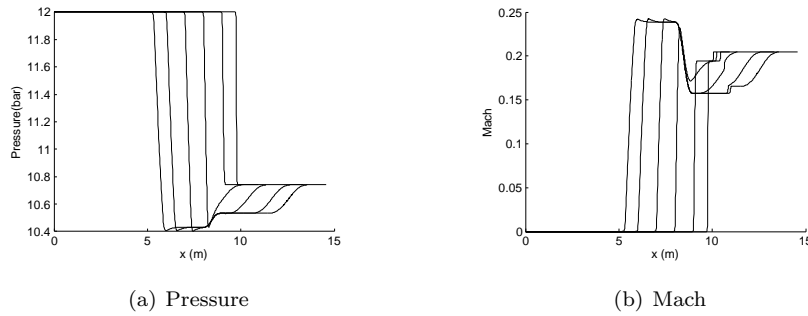
Figure 3.2: Pattern A

For lower value of the area ratio a slightly different behavior occurs, a compression wave was found to form in the area change and then follow the tail of the transmitted fan and decrease is power. Going forward in time the final strength of the transmitted waves should agree with the quasi steady prediction, also in this case the flow that move in the right direction becomes steady quite faster. This deviation from the pattern A is also found for ideal gas flow as reported in [24]. In this case the situation could be very critical, due to the formation of this compression wave in fact the boundary layer could separate.
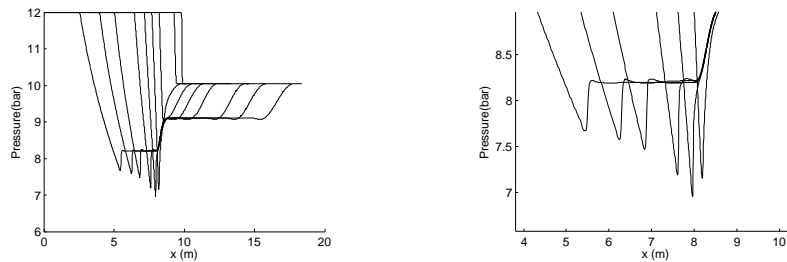
Figure 3.3: Pattern A with shock waves at the tail of the transmitted fan

3.1.2 Geometry definition

Once this short training has been done we could analyze the behavior of the entire facility. The adopted geometry (figure 3.4) is composed of a straight pipe of 16 m, a diverging of 1 m, a test section of 1 m, the cascade has been replaced with a simple nozzle. After the nozzle a large divergent of area ratio 10 has been placed to reproduce the effect of the low pressure plenum, between it and the cascade a small straight pipe has been placed just to place the valve.

Each area change has been modelled with the equation 3.1, the radius of the tube has been chosen 0.04 m, the test section area 0.0218 m^2, the area ratio then is of 0.23. The throat area has been chosen ten times smaller respect to the test section whereas the discharge are eight times bigger respect to the throat. The mesh has been refined near the steep area change with a gaussian function and is composed of 2060 elements.
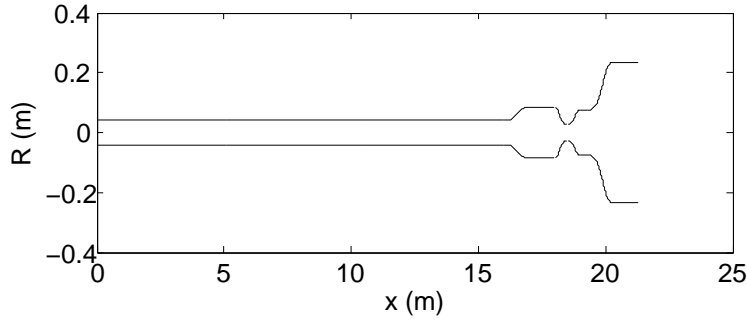
Figure 3.4: Geometry in case of classic set-up with a divergent before the test section (divergent configuration)

The second set-up that has been investigated (figure 3.5) presents a charge tube of equal area to the test section. In this case the geometry is more simple, moreover during the experiment a reflected expansion wave is not expected, for this reason the charge tube could be considerably shorter, also the quality of the flow through the cascade in the real case will be better in fact the perturbations that arise during the area change are not amplified by the divergent.

On the other hand a larger tube involves larger amount of fluid for the experiment (and then larger cost), moreover convective motions could arise before the test affecting thus the experiment. The appropriate decision will be taken in a next phase of the project, scope of this work is just to present the possible configuration.

For this configuration a tube of 7 m and a test section of 1 m have been taken, the area of the tube then has been taken of 0.0218 m^2 then the radius will be 0.08 mm, all the other dimensions have been kept equal to the previous geometry, in this case the mesh is composed of 1160 elements.
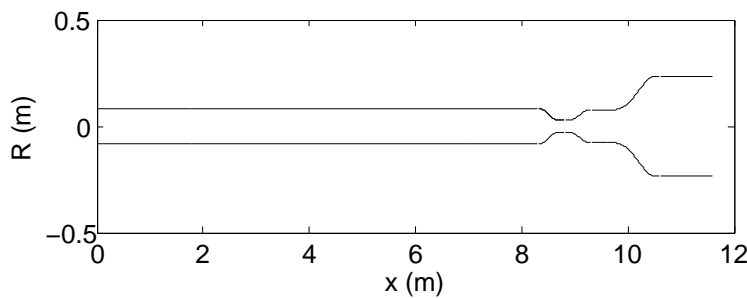
Figure 3.5: Geometry in case of set-up with tube and test chamber of same dimensions (straight configuration)

3.1.3 Results

For both simulations the fluids used is MDM, it is a fluid of considerable low cost widely used in commercial ORC. In order to estimate the test time the evolution of characteristic parameter of a fluid-dynamic experiment at the inlet of the cascade (Mach, Reynolds, compressibility factor and the fundamental derivative of gasdynamics) has been checked.

First configuration In this case we are dealing with a reflected expansion waves travelling in the test section, bouncing between divergent and cascade and losing intensity more and more, therefore each parameter of interest doesn't reach a fixed value but continues to vary more and more slowly until its steady value. In order to obtain a test time estimation a tolerance of 1 % respect to its final value has been fixed for each parameter.

	Left	Right	Inlet
Mach	0.0	0.0	0.07
Pressure (bar)	12	3.11	80.5
Density (kg/m^3)	109.9	22.7	10.1
Temperature ($^{\circ}C$)	287.5	201.3	282.4

Table 3.2: Thermodynamic states of the simulation

(a) Mach

(b) Fundamental derivative

(c) Compressibility

Figure 3.6: Behavior of the adimensional parameter at the inlet of the cascade (the red line refers to a tolerance of 1% respect to the expected solution)

The time needed to the reflected wave to expire depend on its intensity and on the

length of the test section. Since it lose intensity every time that it goes into the diverging or the cascade, the shorter is the test chamber the lower is this time (and consequently the higher is the test time). The inlet thermodynamic states depend clearly on the states in the charge tube but also on the dimension of the facility.

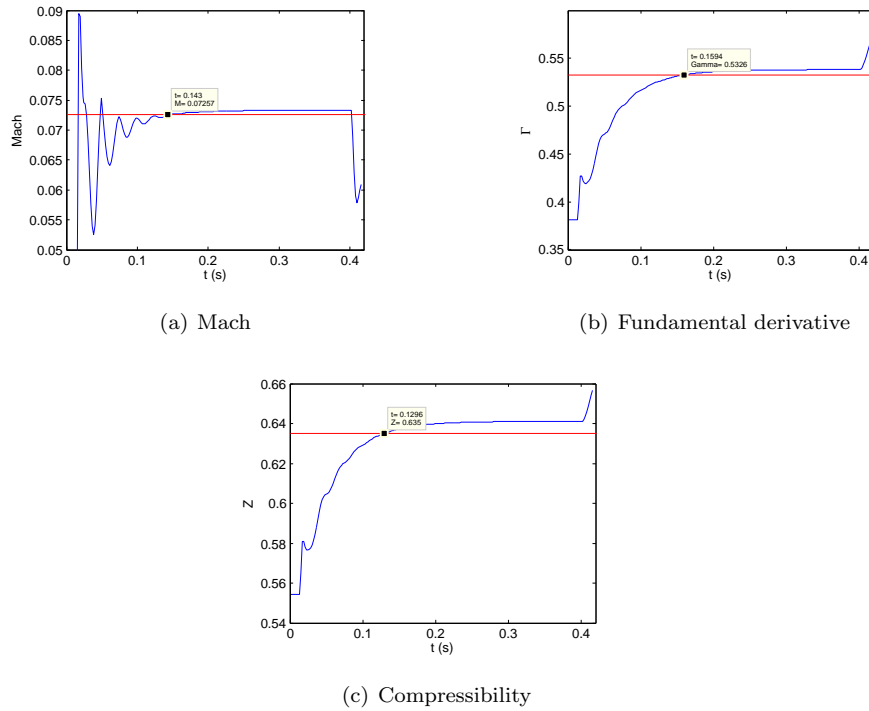The expected time is $0.25 \ s$ it could be considered enough for this kind of experiment, it is very sensitive to thermodynamic condition, fluid used, length of the test section and clearly area ratio between charge tube and test chamber.

It could be interesting to present the pressure profile along the facility at different times. Referring to figure 3.1.3 we could observe that the behavior of the fun through the diverging refers to that expected by the pattern A, however it presents a weak compression wave since the area ratios are quite low, in the low pressure plenum due to the bouncing shocks a lot of perturbations arises, however it can't go through the inlet of the cascade since it is choked.
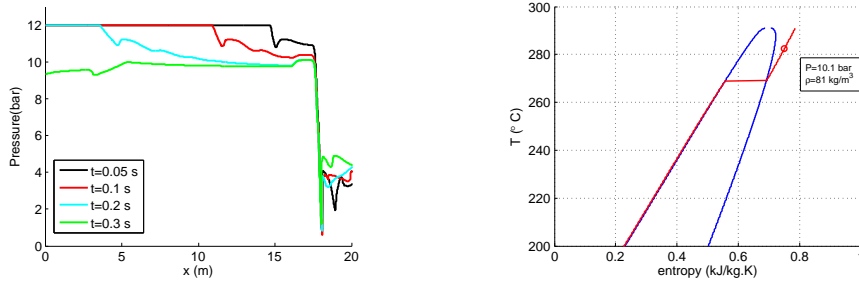
Figure 3.7: Pressure profile at different time along the facility (left) and inlet thermodynamic condition (right)

Second configuration   Without divergent the configuration is much closer to a standard Ludwieg tube, no reflected wave will be formed therefore after the passage of the first expansion wave the test could start, for this reasons the charge tube has been taken shorter, furthermore each thermodynamic quantities reach their steady value after the passage of the expansion wave and then no tolerance is needed for define the test time.

The inlet pressure and density are fixed by the characteristic of the cascade (area ratio between the throat and the inlet), and by the thermodynamic state in the charge tube, and it could be easily predicted by a simple one-dimensional analysis. As in the previous simulation the thermodynamic state in the low pressure plenum doesn't affect the experiment, it is necessary only that the pressure is low enough to chocke the cascade.

In this case three different analyses have been carried for three different organic fluids of increasing molecular complexity, pentane, MDM and PP5.

	Molecular weight	P_{crit} (bar)	T_{crit} $(°C)$
Pentane	72.2	33.7	196.6
MDM	236.5	14.15	290.9
PP5	462	17.9	291.8

Table 3.3: Thermodynamic properties of the fluids

	Left	Right	Inlet
Pentane			
Mach	0.0	0.0	0.07
Pressure (bar)	12	3.11	11.5
Density (kg/m^3)	109.9	22.7	101.7
Temperature $(^\circ C)$	287.5	201.3	285.8
MDM			
Mach	0.0	0.0	0.07
Pressure (bar)	12	3.11	11.5
Density (kg/m^3)	109.9	22.7	101.7
Temperature $(^\circ C)$	287.5	201.3	285.8
PP5			
Mach	0.0	0.0	0.07
Pressure (bar)	12	3.11	11.5
Density (kg/m^3)	109.9	22.7	101.7
Temperature $(^\circ C)$	287.5	201.3	285.8

Table 3.4: Thermodynamic states of the simulations

Looking at the figure 3.8 and at the table 3.5 the useful test time has different values changing the fluid, the reasons is that the speed of sound is very sensitive to the molecular complexity of the fluid, complex and heavy fluids have lower speed of sound and simple and light fluids have higher speed of sound.
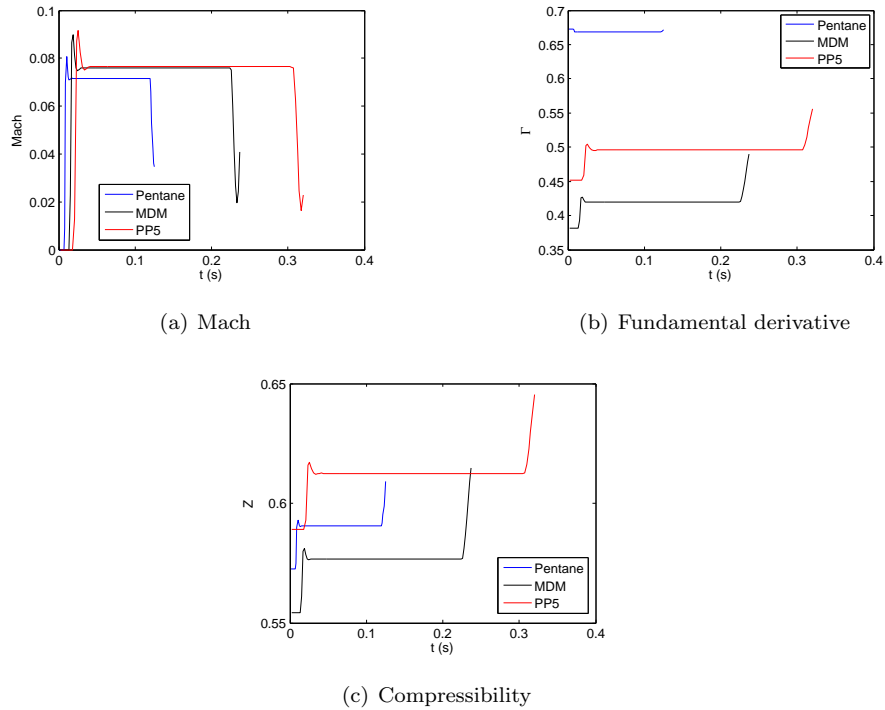

(a) Mach

(b) Fundamental derivative

(c) Compressibility

Figure 3.8: Behavior of the adimensional parameter at the inlet of the cascade

Is well know that the perturbations travel in a fluid at this characteristic speed, then the expansion wave is faster in case of simpler fluid like pentane whereas for more complex fluids is slower.

	Speed of Sound (m/s)	Γ_{inlet}	Test Time (s)
Pentane	140.79	0.67	0.098
MDM	74.32	0.42	0.187
PP5	57.49	0.49	0.252

Table 3.5: Thermodynamic properties of the fluids

The test time could be acceptable for MDM and PP5. For simpler fluids like Pentane it could be better to have a longer tube, it is clear however that this configuration improves the performance of the facility, in fact the charge tube in this case has been taken equal to an half respect to the previous configuration. The amount of fluid needed in these configuration is higher 0.1526 m^3 against only 0.0804 m^3 in the previous configuration, this could be a problem especially considering the opportunity of testing more expensive fluids.

3.2 Two dimensional cascade analysis

Scope of this set of analyses is to predict the flow field at the mid-span of the cascade for different pressure ratio. Results has been compared with periodic solutions on the same blade to evaluate the lack of periodicity brought by the upper and lower walls. Once again the simulation was carried out using zFlow coupled with FluidProp, the flow has been approximated as inviscid and steady.

3.2.1 Geometry definition

Once again the investigated blade is the Biere, it has been designed by a private manufacturer for MDM based ORC, it has been used for this simulations as well as for the periodic simulations coming from [37]. The passage, as shown in figure 3.9, has been designed without the use of an accurate two-dimensional real gas CFD simulation tool, it should be also noted that in the figure the aspect ratio is distorted, because the turbine design is confidential property of the manufacturer.

The simulation of a finite cascade respect to a standard periodic simulation presents the problem of the inclination of the upper and lower wall. The behavior of the flow over a finite cascade, more than the back-pressure imposed as boundary condition, depends in this cases on the orientation of the tailboard.

The adopted procedure consists into the identification of the streamlines coming out from the trailing edge of one blade of a chosen periodic simulation and its interpolation with the lasts square technique. With this procedure the upper and lower wall of the cascade for a given thermodynamic condition are created. Once the proper inclination of the tailboard has been fixed the geometry is defined. The meshes have been made with the commercial software Gambit, they are made of around 28000 triangular elements,since the simulations are inviscid, no refinement is needed near the boundary.
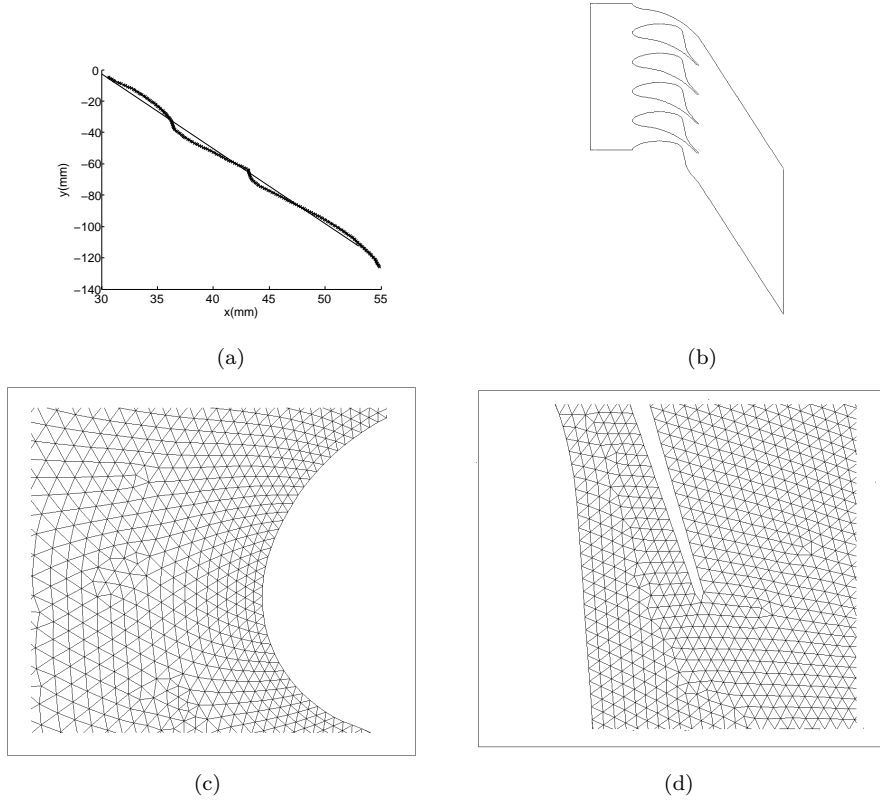
(a)

(b)

(c)

(d)

Figure 3.9: (a) lasts square interpolation of a streamline, (b) cascade geometry, (c-d) particular of the mesh of the blade.

Three different simulations have been carried out (table 3.6), the fluid used is MDM (since the Biere blade has been designed for working with it), two are at subcritical inlet conditions with different value of pressure ratio, the last is at supercritical inlet conditions. On the upper and lower wall as over the blades non-penetration condition has been imposed.

An optimal convergence rate is obtained using the implicit backward Euler integration scheme, the CFL number has been automatically handled by the code, all flow solutions are converged up to the six orders of magnitude of the all conserved variables, moreover the second order of accuracy has been reached.

	Design point	Part load	Supercritical
P_{01}/P_2	6	4	4.15
$P_{01}(bar)$	8	8	18
$T_{01}(^\circ C)$	270.5	270.5	304.6
Z_{01}	0.72	0.72	0.26
$P_2(bar)$	1.33	2	4.33
Z_2	0.96	0.93	0.86

Table 3.6: Thermodynamic condition of the simulations

3.2.2   Results

Design point   The stator passage has been designed for the design point conditions presented in table 3.6, the periodic solution (figure 3.10 right) present a weak shock coming out from the blade trailing edge and hit on the blade below, in the finite cascade (as in the test section) this shock bounces against the tailboard and comes back through the cascade disturbing the flow field.
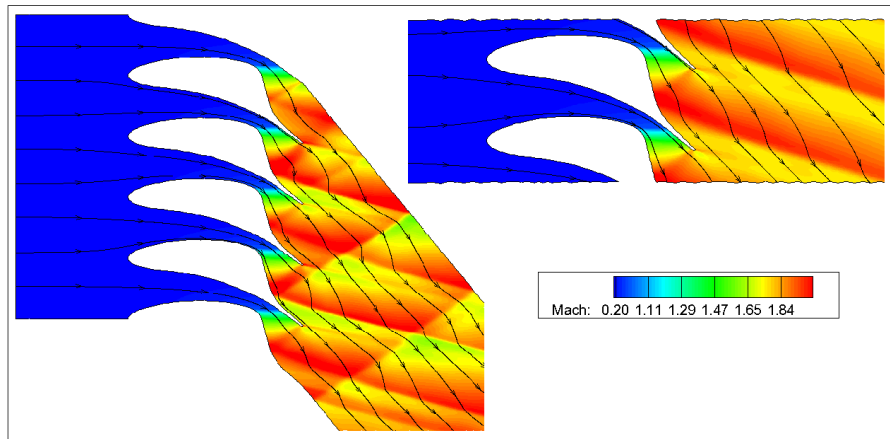
Figure 3.10: Periodic and cascade CFD simulation (design point)

This effect is clearer highlighting the density gradient and so the shock wave (like in a Schlieren visualization). Looking at figure 3.11 the shock wave bouncing on the tailboard after the blade 1 disturbs the outflow field of blade 2 and hits on the blade three. It is clearly the responsible of the difference in the flow field between the two simulations since no other possible effects of disturbance as turbulence, boundary layer or three-dimensional effect are reproduced in this simulations.

Figure 3.11: Numerical Shlieren visualization of the flow field

In figure 3.2.2 the Mach number and the pressure along the boundary of the blade is plotted in term of the reduced coordinate S/C (starting from the leading edge) for the periodic simulation and for three blade of the cascade. The result is in good agreement for

the suction side and for the first part of the pressure side, however near the blade trailing edge the incoming shock wave introduces quite relevant deviations.

(a) Mach

(b) Mach

(c) Pressure

(d) Pressure

——	periodic simulation pressure side
—*—	periodic simulatio suction side
—*—	blade cascade suction side
——	blade cascade 1 pressure side
——	blade cascade 2 pressure side
——	blade cascade 3 pressure side

Figure 3.12: Difference between periodic simulation and cascade simulation in term of Mach and pressure along the boundary of the blade

Looking at figure 3.13 it's clearer the effect of the spurious shock waves, in cases of channel 1 and 3 it affects the Mach outflow profile introducing a weak spurious decreases in the upper part of the outflow line and increasing the effect of the trailing edge shock wave. Channel 2 is not hit by spurious shock wave, it in fact passes just downstream and this produces a better match with the periodic simulation.

(a) Mach   (b) Pressure

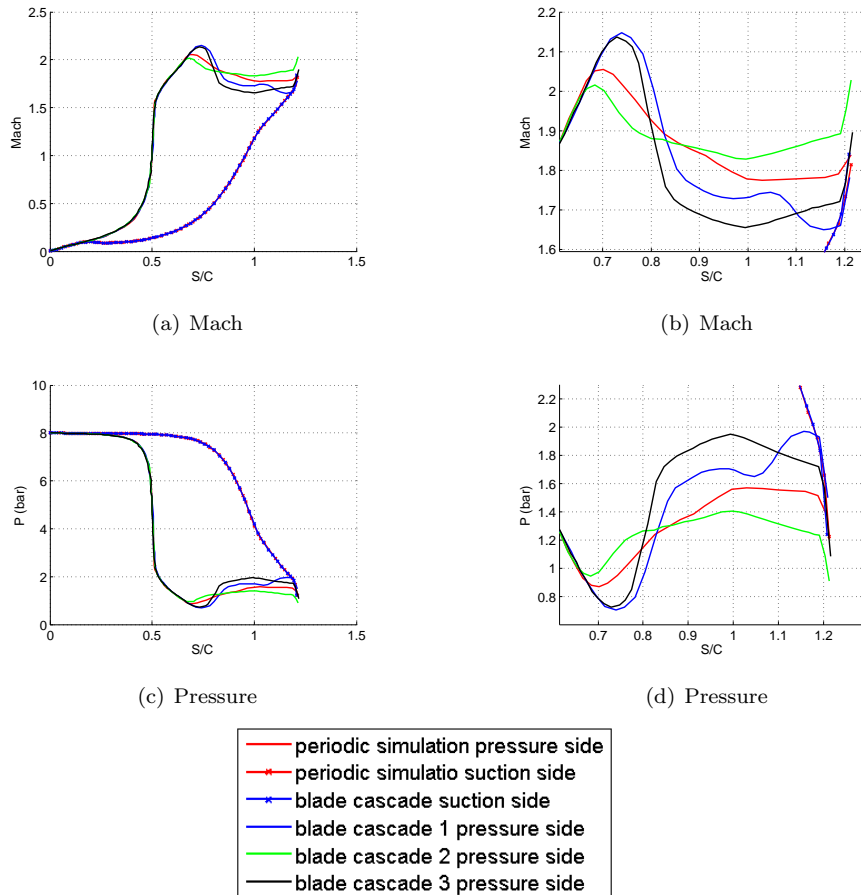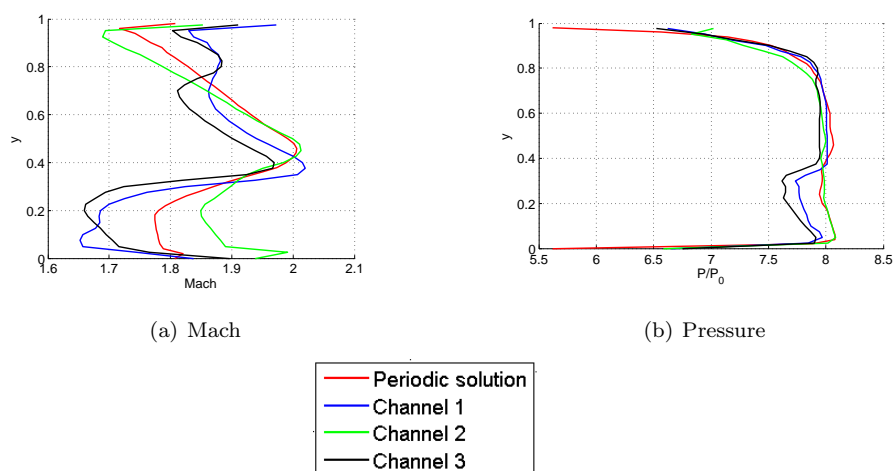Figure 3.13: Difference between periodic simulation and cascade simulation in term of Mach and pressure along the outflow line (in this case the number refers to the upper channel of the blade of interest)

The pressure loss coefficient (CPL= $1 - P_{02}/P_{01}$) quantify the loss in pressure due to the presence of shock wave, it is a good indicator for a turbine blade, in table 3.7 the difference in the mass weighted CPL between different simulations are reported, in case of the central channel the agreement is good, in channel 1 and 3 the shock wave produces a higher decrease of total pressure.

	Design Point	Part Load	Supercritical
CPL periodic	0.0218	0.0496	0.0870
CPL cascade 1 (% error)	0.0250 (14.5)	0.0536 (8.1)	0.0572 (-29.4)
CPL cascade 2 (% error)	0.0221 (1.2)	0.0682 (37.6)	0.0601 (-28.1)
CPL cascade 3 (% error)	0.0315 (44.3)	0.0551 (11.1)	0.0626 (-26.2)

Table 3.7: Mass weighted pressure loss coefficient for periodic and cascade simulation and percentage error for the three central channel

Part-Load   Because ORCs can operate at part-load conditions, the associated performance is important, the inlet total pressure has been kept fixed, whereas the pressure ratio has been reduced to 4. Again as in the previous simulation the outflow is disturbed by the shock wave coming from the upper boundary (figure 3.14).

In this case spurious shock is stronger since we are dealing with part load condition, spurious shock waves hit blade 2 and 3, clearly as we have seen in the previous figure all the cascade is affected by these disturbances, then keeping low these effects is necessary to achieve good results during the experiment. As anticipated before a widely used technique is using porous tailboard, looking at the results of this simulations these is strongly recommended during the experiment.
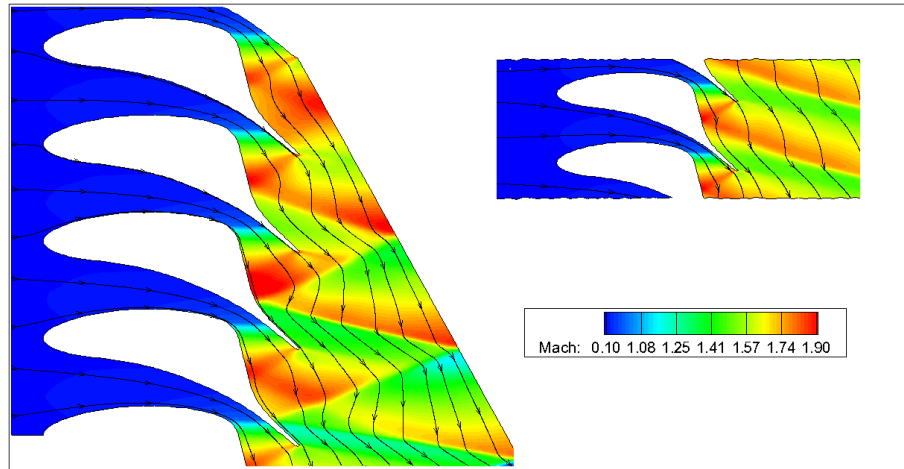
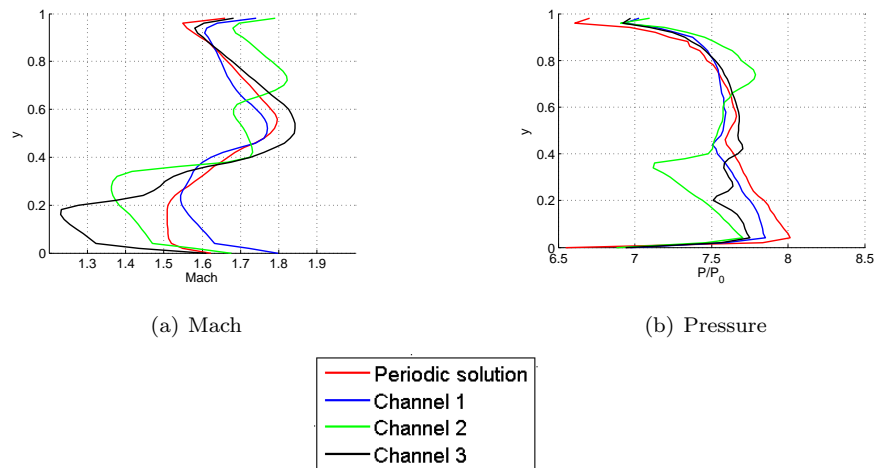Figure 3.14: Periodic and cascade CFD simulation (part load)

| (a) Mach | (b) Pressure |

Figure 3.15: Difference between periodic simulation and cascade simulation in therm of Mach and pressure along the outflow line (trailing edge-trailing edge)

Since the shock waves are stronger also the differences in term of CPL are greater. The best match is achieved by channel 1, however it is necessary point out that during an experiment the measurement channel in this cascade is number 2, this because other factors like end-wall boundary layer introduce disturbances that are stronger for channel 1 and 3 since they are more closer to upper and lower wall.

Supercritical The supercritical configuration simulation (figure 3.16) presents a substantial difference respect to part load and design point. The pressure loss coefficient in fact in the first two simulations presents, as expected, higher values in case of the cascade simulation, the spurios shock wave in fact introduces larger decreases in total pressure.
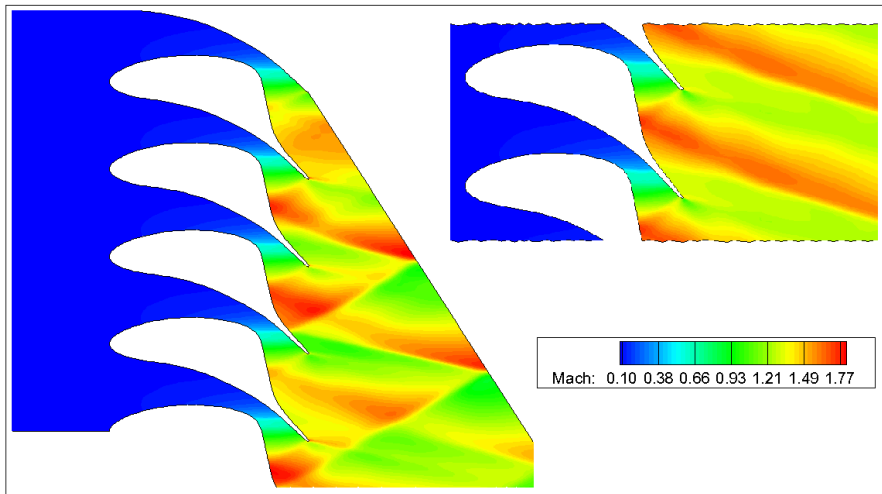
Figure 3.16: Periodic and cascade CFD simulation (supercritical condition)

(a) Mach
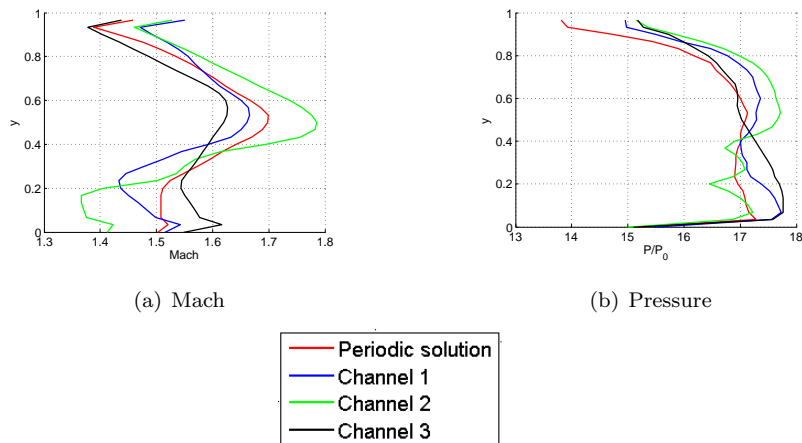
(b) Pressure

Figure 3.17: Difference between periodic simulation and cascade simulation in therm of Mach and pressure along the outflow line (trailing edge-trailing edge)

In this case the CPL for cascade simulation is much lower, in case of channel 3 the reason is that no shock travels through the outflow line, in case of channel 1 and 2 the reason is that after the shock the density and the pressure increases much more and the module of the velocity decreases less than in the periodic case because of the change in thermodynamic behavior of MDM.

This is clear comparing the outflow profile of the fundamental derivative of gasdynamics (figure 3.18) in case of design point simulation and supercritical simulation, in this last case the value of Γ for channel 1 and 2 reaches lower value, that means a different behavior that reflects to an underestimation of the CPL.

(a) Design point (b) Supercritical
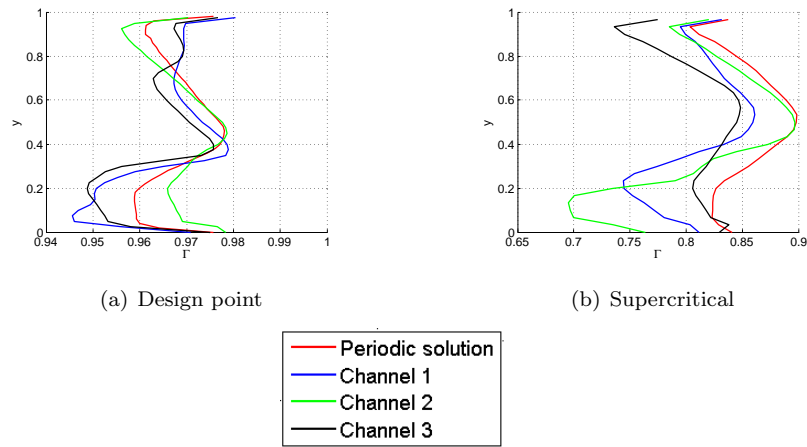
Figure 3.18: Difference design point simulation and supercritical simulation in term of Γ along the outflow line (trailing edge-trailing edge)

3.3 PIV measurements

The facility has been primarily designed to develop flow field measurements through the PIV technique [34]. This technique providing instantaneous velocity vector measurements in a cross section of the flow. Two velocity components are measured, the use of modern digital cameras and dedicated computing hardware results in a real time velocity map.

Figure 3.19: Typical Particle Image Velocimetry set-up

In PIV, the velocity vectors are derived from sub-sections of the target area of the particle-seeded flow by measuring the movement of particles between two light pulses. The target area is called field of view (F.O.V.) and it is the area recorded by the camera, it is divided in sub-section called interrogation area.

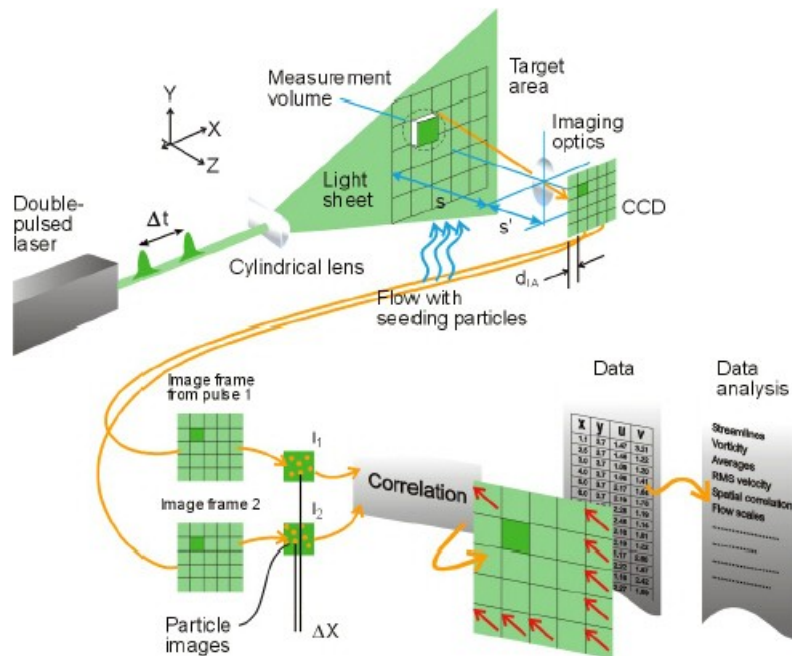Once that a particle is lighted by the light sheet a physical phenomenon called scattering occurs, the light scattered (reflected) by each particle is recorded by a CCD camera that is able to capture each light pulse in a separate image frame.

Once a sequence of two light pulses is recorded, the images are divided into small subsections called interrogation areas (IA). The interrogation areas from each image frame, I_1 and I_2, are cross-correlated with each other, pixel by pixel. The correlation produces a signal peak, identifies the common particle displacement (to improve the accuracy in the computing of the displacement a sub-pixel interpolation technique is often used).

A velocity vector map over the whole target area is obtained by repeating the cross correlation for each interrogation area over the two image frames captured by the camera. In case of measurement of a steady and controlled flow average is done between different realizations improving the accuracy of the measurements.

In the following we outlined some advantages that making particle image velocimetry a leading measurement technique:

- large non intrusive, the tracer particles generally causes negligible distortion in the fluid flow

- it is a method capable of measuring the entire two-dimensional flow field simultaneously

- high speed data processing allows the generation of large number of image pairs which may be analyzed in real time or at a later time and a high quantity of near-continuous information may be gained

- sub-pixel displacement values allow high degree of accuracy

Schlieren Shadowgraphy Schlieren flow visualization is based on the deflection of light by a refractive index gradient. The index gradient is directly related to flow density gradient. The deflected light is compared to undeflected light at a viewing screen, the undisturbed light is partially blocked by a knife edge, that light produces a shadow pattern depending upon whether it was previously blocked or not. This shadow pattern is light-intensity representation of the expansions and compressions which characterize the flow.

3.3.1   Particle response

As anticipated before the particles have to follow the fluid as best as possible, in presence of shock sharp decreases in velocity occur, therefore this is the most critical (but also one of the most important) condition for the particles.

Since the particle density exceeds the fluid density by several orders of magnitude, the motion of a particle inside a fluid is dominated by the viscous drag, however the complex equation of motion of a particles [38] could be approximated as:

$$\frac{dU_p}{dt} = \frac{U - U_p}{\tau} \tag{3.2}$$

where τ is the relaxation time of the particle (equation 2.2).

In order to have an estimation of the drag coefficient for a spherical particle Tedeschi et al. in [39] presented several methods for different values of the Knudsen number of the particle. It has defined as:

$$Kn = \frac{d_p}{\lambda} \tag{3.3}$$

where λ is the mean free path of the molecules of the working fluids.

$$\lambda = \frac{K_b T}{\sqrt{(2\pi)} d_{hs}^2 P} \tag{3.4}$$

where K_b is the Boltzmann constant and sigma is the diameter of the molecule. The diameter of an MDM molecule could be computed with the hard sphere approximation, following [40]:

$$d_{hs} = \sigma(1 - 0.12 exp(-3\epsilon/kT)) \tag{3.5}$$

where $\epsilon/k = 213K$ is the segment energy parameter and $\sigma = 0.41689nm$ is the segment diameter.

At this point we can compute the particle drag coefficient, the TiO_2 particles have a nominal diameter of $d_p = 400nm$ and a bulk density of $\rho_d = 200Kg/m^3$ the Reynolds number based on the diameters of the particle is:

$$Re_d = \frac{\rho U d_p}{\mu} \tag{3.6}$$

The particle drag coefficient is defined by:

$$C_D = \frac{24}{Re} k(1 + 0.15(k * Re)^{0.687})\xi(Kn)C \tag{3.7}$$

$$\xi(Kn) = 1.177 + 0.177\frac{0.851Kn^{1.16} - 1}{0.851Kn^{1.16} + 1} \tag{3.8}$$

$$C = 1 + \frac{Re^2}{Re^2 + 100}e^{-0.225/M^{2.5}} \tag{3.9}$$

$$k = (1 + \frac{9}{2}Kn)^{-1} \tag{3.10}$$

where $xi(Kn)$ is an expression that extend the range of validity of the equation in the free molecule flow, C is a correction factor valid for $\Delta M > 0.3$ and k is the slip coefficient evaluated with the Cunningham's law (this could be a good approximation for $Kn > 1$).

Once the C_d the relaxation time could be calculated, multiply it for the velocity before the shock we obtain the particle relaxation length that is the distance that the particle needs to return in equilibrium with the fluids.

The result obtained for this analysis are presented in table 3.9 and the reference state coming from the simulation previously presented are reported in table 3.8, here the state A refers upstream to the shock while the state B refers downstream to the shock.

| | P.L. | | D.P. | | Sup. | |
	A	B	A	B	A	B
Mach	1.96	1.75	1.76	1.48	1.7	1.5
Temperature ($^\circ C$)	249.9	286.6	249.1	255.7	259.5	267.4
Pressure (bar)	1.10	1.52	1.49	2.48	3.23	4.92
Velocity (m/s)	269.04	226.72	228.30	186.51	208.56	173.35
Viscosity ($Pa*s*10^6$)	9.3	9.9	9.3	9.6	9.2	9.5

Table 3.8: Reference state for the estimation of the particle response

	ΔM	$d_{hs}(nm)$	$\lambda(\mu m)$	Kn	Re_d	C_d	$\tau(\mu s)$	$\xi(mm)$
D. P.	0.21	0.3411	0.2192	1.824	67.29	0.0753	0.8508	0.22
P. L.	0.28	0.3416	0.1646	2.430	84.49	0.0677	0.7531	0.17
Sup.	0.20	0.3427	0.0515	7.769	232.52	0.0058	3.17	0.55

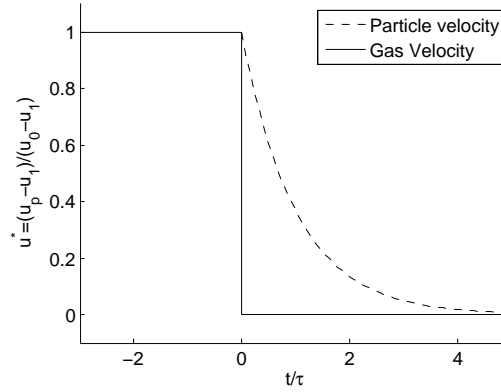Table 3.9: Relaxation time computation

Figure 3.20: Particle response to a normal shock wave

In compressible flow a velocity change is coupled by a temperature change. Therefore the particle occurs also in a temperature lag. The time rate of change is given by [41]:

$$\frac{\pi d_p^3}{6}\rho_p c\frac{dT_p}{dt} = h\pi d_p^2(T - T_p) \tag{3.11}$$

where c is the thermal capacity of the particle material $c = 712j/kgK$ and h is the heat transfer coefficient. This could be rewritten in order to obtain the temperature relaxation time:

$$\frac{dT_p}{dt} = \frac{T - T_p}{\tau_T} \tag{3.12}$$

Where the temperature relaxation time is:

$$\tau_T = \tau\left(\frac{1}{8}\frac{Prc_dRe_d}{Nu}\frac{c}{c_p}\right) \tag{3.13}$$

Starting from the thermodynamic condition used for the calculation of the relaxation time and calculating all the required thermodynamic properties with FluidProp ,we assume a conservative $Nu = 2$ (pure conduction) obtaining a temperature relaxation time of respectively:

$$\tau_T = 0.0793\mu s \tag{3.14}$$

$$\tau_T = 0.0782\mu s \tag{3.15}$$

$$\tau_T = 0.0750\mu s \tag{3.16}$$

Considering Stokes drag ($24/Re_d$) in spite of 3.7 a more conservative temperature relaxation time has been obtained, $\tau_T = 0.3652\mu s$, $\tau_T = 0.3281\mu s$ and $\tau_T = 1.3272\mu s$ in all cases it shows that the particle will be in thermal equilibrium with the gas flow downstream of the shock.

Since all the values could be considered some way lower supercritical simulation requires particular attention, in this case the values are considerably larger respect to the other. This value has to be clearly verified in a more accurate experimental way before starting any test over ORCs blade cascade.

It is useful to have a comparison with a PIV experiment in air [14], for a stronger shock (relative Mach number $\Delta M = 0.7$) the Knudsen number is $Kn = 1.2$, the drag coefficient $C_d = 2.2$, the Reynolds number based on the particle diameter $Re_d = 4.8$ and the Prandtl number $Pr = 0.72$. This results in a particle relaxation time of $\tau = 1\mu s$ and a temperature relaxation time of $\tau_T = 0.75\mu s$.

3.3.2 PIV performance

In order to obtain more accurate measurements of the flow field it is necessary to record different realization of the flow field and doing the ensemble average on it. For this procedure is necessary to extract n pairs of image of the flow field, doing the cross-correlation between each pairs obtaining n different realization and finally doing the average between the n velocity field.

Knowing the characteristics of the CCD camera and the useful run time of the experiment it is possible to roughly obtain how many runs are necessary for having an accurate evaluation of the flow field. The equipment avaiable at the the TU Delft P&E department is a Pco.dimax digital high speed 12 bit CMOS camera, the main characteristics are:

- Resolution: 2016 x 2016 pixel

- Frame rate: 1100 fps @ 2016 x 2016 pixel or 4000 @ 1032 x 1024 pixel

- Exposure time range: 2 μs - 1 s

The frame rate is the number of images that the camera could record in one second, for obtaining one realization of the flow field two images are needed therefore at full resolution 550 realization could be obtained in 1 second of steady flow. Taking a nominal run time of 0.1 seconds we obtain 55 different realizations of the flow field for each run.

It's interesting to point out that using steam for this kind of facility is possible to obtain only 5-10 realizations of the fluids for each run.

Thanks to the high quality of the camera and to the low sounds speed of the organic fluids adopted only one run is necessary to obtain a sufficiently large sample for doing an accurate statistical analysis.

The field of view together with the resolution of the camera determine the smallest resolved flow structure. The field of interest is one channel between two blades and the discharge area downstream of it. However during a test it is possible to focus only on one of these two main areas to achieve higher resolution.
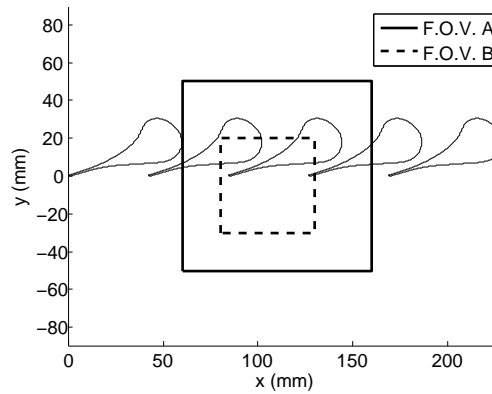

Figure 3.21: Field of view: A 10x10 cm, B 5x5 cm

In figure 3.21 two possible fields of view are drawn over the cascade. At full resolution of the camera 2kx2k pixels, with a typical interrogation window of 32x32 pixels the smallest resolved flow structure are (2000pixel/32pixel=62.5):

- 100 mm/62.5=1.6 mm

- 50 mm/62.5=0.8 mm

Chapter 4

Conclusions & Perspectives

4.1 Conclusion

A preliminary design for a test-rig for turbine blade to be operated in ORC cycles was drafted. The facility is a modification of an existing facility FAST [36], used mainly for detecting of rarefaction shock waves. The expected facility characteristics are as follows: test time up to 0.25 s, number of blades 5 to 7, test section dimension 125x170 mm.

The total conversion efficiency of ORCs is dependent on the efficiency of its components. Experimental tests over ORCs turbine blade are almost totally absent in the scientific scenario, then developing an experimental facility of this kind could significantly improve the design of such important components.

First of all it is necessary that the facility covers a wide range of working fluids, from more commercial like MDM or toluene to more scientific like D6 or D4 that could results more efficient. This is mainly related to the dimension of the charge tube and its length and clearly it is a trade off between cost and benefits. Another important point is the quality of the flow in the test section, in this case the divergent is the key part and therefore the area ratio between the inlet cascade area and the charge tube cross section.

In this view there are some devices that seem to be necessary. Looking at the comparison between periodic and cascade CFD simulation, huge differences coming from the reflection of the shock wave, this is a peculiarity of this kind of blades with outflow Mach number of ≈ 1.7 to be compared with ≈ 1.2 of standard supersonic steam cascade they could generate stronger shock waves. Porous tailboard is the device that could reduce this problem but its requires an accurate study in order to decide the optimal ratio between holes and solid wall. Another important device is a boundary layer suction system, in this cases it is widely used in wind tunnel and it could be easily implemented by making a connection between the test section and the low pressure plenum.

PIV technique seems suitable with dense gas test,however, if its use is well known with Ludwieg Tube type facility, it's not yet verified with this kind of gas, therefore a step by step procedure could be necessary and the Schlieren Shadowgraphy could be useful also in this view. In this sense a key point is the repeatability of the experiment, from this point the proposed configuration could be better respect to a standard blowdown configuration since a lower amount of fluid is required, another advantage is the cost both in term of build and in term of test.

In conclusion this facility seems particularly suitable for studying the behavior of ORC turbine blade, it will support optimization work and it could also validate CFD program

and thermodynamic library improving the existing ORCs cycle and studying new possible configuration and working fluids.

4.2   Perspectives

The work to build up a facility of this kind is certainly much, as first of all it is is necessary to decide which configuration is better to adopt. For this decision it could be useful carry on a simulation of the flow field in the two configurations, with or without divergent.

A study of the convective mote into the charge tube due to the gradient temperature and a study of the perturbation introduced by the divergent would help to make a decision, the geometry is very simple but this type of problem are turbulent and three-dimensional and then are not easy tasks. This decision cannot ignore cost consideration, then an accurate estimation on the cost in term of building materials and cost for doing an experiment is very useful.

In this way is necessary to find how to purify the working fluids by the particle after each experiment, in classic PIV experiment with air it is not necessary since the amount of fluids under test is simply replaced with other clean air. In case of organic working fluids, this will cause an exponential increase in the cost of an experiment therefore finding a way to remove this particle allow us to use the same amount of fluid for more tests.

Once these decisions have been taken the overall geometry of the facility is decided and the complex building process can start.

Acknowledgments

Bibliography

[1] H.M. Curran. *Use of Organic Working Fluids in Rankine Engines.* Journal of Energy, 5(4):218-223, 1981.

[2] G. Angelino, M. Gaia, and E. Macchi. *A review of Italian activity in the field of organic Rankine cycles.* In VDI Berichte - Proceedings of the International VDI Seminar, volume 539, pages 465-482, Dusseldorf, 10-12 September 1984. VDI Verlag.

[3] Schuster A. Karellas. *Supercritical fluid parameters in organic rankine cycle applications.* International Journal of Thermodynamics, 11(3):101-108, 2008.

[4] G. Angelino, P. Colonna. *Multicomponent working fluids for Organic Rankine Cycles (ORCs).* Energy, 23(6):449-463, 1998.

[5] J. Larjola. *Electricity from industrial waste heat using high-speed organic Rankine cycle (ORC).* Int. J. Prod. Econ., 41(1-3):227-235, October 1995.

[6] G. Angelino, P. Colonna. *Organic Rankine cycles for energy recovery from molten carbonate fuel cells.* In 35th Intersociety Energy Conversion Engineering Conference (IECEC), number 2000-3052, pages 1-11. AIAA, July 2000.

[7] G. Angelino, P. Colonna. *Air cooled siloxane bottoming cycle for molten carbonate fuel cells.* In Fuel Cell Seminar, pages 667-670, October 2000.

[8] M. Brentegani. *A μ-ORC system for domestic cogeneration.* M.Sc. Thesis ET-2389, Politecnico di Milano - Delft University of Technology, July 2009.

[9] G. Angelino, C. Invernizzi. *Real gas Brayton cycles for organic working fluids.* Proceedings of the Institution of Mechanical Engineers, Part A: Journal of Power and Energy, 2001.

[10] G. Angelino, C. Invernizzi. *Prospects for real gas reversed Brayton cyclesheat pumps.* Int. J. Refrig., 18:272, 1995.

[11] P.A. Thompson. *A fundamental derivative in gasdynamics.* Phys. Fluids,14(9):1843-1849, 1971.

[12] P. Colonna, A. Guardone. *Molecular interpretation of nonclassical gasdynamics of dense vapors under the Van der Waals model.* Phys.Fluids 18, 056101, 2006.

[13] H.Ludwieg. *Zeitschrift fur Flugwissenschaften* Der rohrwindkanal 3:206-216, 1955

[14] F.F.J.Schrijer *Experimental investigation of re-entry aerodynamic phenomena* PHD thesis, TU Delft, 2010

[15] N.C.Bainse, M.L.G. Oldfield, T.V. Jones, D.L. Schultz, P.J.King, L.C. Daniels *A short duration blowdown tunnel for aerodynamics studies on gas turbine blading* ASME paper 82-GT312, 1982.

[16] A. Spinelli, V. Vandecauter, A. Guardone, V. Dossena. *Nozzle design for an organic vapor wind tunnel.* ASMEJ.Turbomachinery,2009

[17] H. Heinemann. *The Test-Facility for Rectilinear Cascades (EGG) of the DFVLR.* DFVLR Bericht IB 222 - 83 A 14, 1983

[18] J. Harinck. *Super-and Transcritical fluid expansions for next generation energy systems.* PhD thesis, TU Delft, 2010.

[19] J. Harinck, P. Colonna, A. Guardone. *Influence of Thermodynamic Models in Two-Dimensional Flow Simulations of Turboexpanders.* Journal of Turbomachinery Vol. 132 011001-1 January 2010

[20] P. Colonna, N.R. Nannan,A. Guardone, E.W. Lemmon *Multiparamter equation of state for selected siloxane* Fluid Phase Equilibria, 244 (2006), 193-211

[21] P.Colonna, S.Rebay *Numerical simulation of dense gas flows on unstructured grids with an implicit high resolution upwind Euler solver* Int. J. Numer. Meth. Fluids Vol.46, 735-765, 2004

[22] AIAA. *Guide for the verificatin and validation of CFD simulations* AIAA-g-077-1998, Reston, VA, 1998

[23] L. Quartapelle, F. Auteri *Fluidodinamica.* Appendice Q, Novembre 2009.

[24] J.J. Gottlieb, O. Igra *Interaction of rarefaction waves with area reductions in ducts* J.Fluid Mechanics, 137:185-305, (1983)

[25] P.Colonna, T. Van Der Stelt *FluidProp: A program for the estimation of thermophysical properties of fluids.* Technical report, Energy Technology Section, Delft University of Technology, 2005

[26] J.F. Louis *Short Duration Experimental Techniques in Turbomachines* Advanced Testing Techniques in Turbomachines, VKI, LS 78 vol. II, 18-04-1975

[27] R. Kiock, F. Lehthaus,N. Baines ,C.H. Sieverding. *The Transonic Flow trough a Plane Turbine Cascade as Measured in Four European Wind Tunnels* J.Engineering for Gas Turbines and Power, Vol 108, No 2, April 1986

[28] C. H. Sieverding. *Advanced methods for cascade testing.* NATO Research and Technology Organisation, AGARDograph 328, AGARD-AG-328, August 1993

[29] D.B.M. Jouini,S.A. Sjolander,S.H. Moustapha. *Aerodynamic performance of a transonic turbine cascade at off-design conditions.* ASMEJ.Turbomachinery,2001

[30] B.H. Goethert. *Transonic Wind Tunnel Testing.* AGARDograph no. 49

[31] A. Rona ,J.P. Gostelow. *Performance of Slotted End Wall Linear Cascade Tunnels at Off-Design Conditions.* AIAA paper, Leicester, 2005

[32] A. Rona,R. Paciorri,M. Geron. *Design and Testing of a Transonic Linear Cascade Tunnel with Optimized Slotted Walls.* Journal of Turbomachinery, Vol. 128/23, 2005

[33] A. Rona,J.P. Gostelow,R. Paciorri,M. Geron. *Wall interference in the discharge flow in a linear cascade wind tunnel.* AIAA 2003-0455

[34] C. Willert, S. Wereley, J. Konpenhans. *Particle Image Velocimetry: A Pratical Guide.* Springer, 2007

[35] D. Ragni, F. Schrijer, B.W. van Oudheusden,F. Scarano. *Particle tracer response across shocks measured by PIV.* Experiment of Fluids, Vol. 50/53-64, 2011

[36] N.R.Nannan, C. Zamfirescu, P. Colonna. *Detailed design pf the flexible asymmetric shock tube (FAST) facility at the P&E department of the Delft University of Technology.* Technical Report ET-2263, TU Delft (2007)

[37] P.Colonna, J.Harinck, S.Rebay, A.Guardone. *Real-gas effect in organic rankine cycle turbine nozzles.* J. of propulsion and power, 24-2, 2008.

[38] A. Melling. *Tracer particles and seeding for particle image velocimetry.* Meas.Sci.Tecnol.,8:1406 - 1416, 1997.

[39] G. Tedeschi, H. Gouin, M. Elena. *Motion of tracer particles in supersonic flows.* Experiment in Fluids, 26:288-296, 1999.

[40] N.A. Lai, M. Wendland, J. Fischer *Description of linear siloxanes with PC-SAFT equation.* Fluid Phase Equilibria, 283: 22-30, 2009.

[41] G. Rudinger. *Flow of solid particle in gases.* Technical Report AG-222,AGARD, 1976.

[42] R.J. Adrian. *Dynamic ranges of velocity and spatial resolution of particle image velocimetry.* Meas. Sci. Technol., 8:1393-1398, 1997